We are IntechOpen,
the world's leading publisher of
Open Access books
Built by scientists, for scientists

6,900
Open access books available

184,000
International authors and editors

200M
Downloads

154
Countries delivered to

Our authors are among the

TOP 1%
most cited scientists

12.2%
Contributors from top 500 universities

BOOK CITATION INDEX
CLARIVATE ANALYTICS
INDEXED

WEB OF SCIENCE™

Selection of our books indexed in the Book Citation Index
in Web of Science™ Core Collection (BKCI)

Interested in publishing with us?
Contact book.department@intechopen.com

Numbers displayed above are based on latest data collected.
For more information visit www.intechopen.com

Ethanol Reforming in the Dynamic Plasma - Liquid Systems

Valeriy Ya. Chernyak[1] et al.[*]
Taras Shevchenko National University of Kyiv
Ukraine

1. Introduction

Today hydrogen (H_2) is considered as one of the most perspective energy sources for the future that can be renewable, ecologically clean and environmentally safe. The demand for hydrogen energy has increased tremendously in recent years essentially because of the increase in the world energy consumption as well as the recent developments in fuel cell technologies. The Energy Information Administration has projected that world energy consumption will increase by 59% over the next two decades, and the largest share will still be dominated by fossil fuels (EIA, 2011).

The interest to alternative fuels research in the last two decades is increased by the depletion of the traditional fossil fuels. Today, ethanol is considered the most perspective fuel for internal-combustion engines (Kakami, 2010).

Alcohols are especially appealing as primary fuels for fuel processors because they can be obtained from renewable biomass: methanol trough gasification and synthesis, and ethanol trough fermentation. Ethanol is easier and safer to store and transport due to its low toxicity and volatility, it is biodegradable, and since water is also consumed during its conversion into hydrogen, there is no need for absolute ethanol to be produced as it would be required if it were to be used in conventional engines, either alone or mixed with gasoline.

Among possible technologies for H_2 production, including steam reforming and partial oxidation of liquid hydrocarbons, the low-temperature plasma reforming of biomass-derived ethanol (ethyl alcohol C_2H_5OH) is believed to be a good alternative approach (Bromberg, 2006). There are various electric-discharge techniques of plasma conversion of ethanol into H_2 using thermal (equilibrium) and non-thermal (non-equilibrium) plasmas: arc, corona, spark, MW, RF, DBD, etc. (Matveev, 2007; Petitpas, 2007). Each plasma system has its merits and demerits, and even difficult to compare. Among them, one of the most efficient is the plasma processing in the dynamic plasma-liquid systems (PLS) using the DC and pulsed electric discharges in a gas channel with liquid wall (DGCLW) and the DC discharge in a reverse vortex gas flow of Tornado type with a "liquid" electrode (TORNADO-LE). Advantages of this technology are high chemical activity of plasma and

[*] Eugen V. Martysh[1], Sergei V. Olszewski[1], Vitalij V. Yukhymenko[1], Sergei M. Sidoruk[1], Oleg A. Nedybaliuk[1], Iryna V. Prysiazhnevych[1], Anatolij I. Shchedrin[2] and Dmitry S. Levko[2]
[1]*Taras Shevchenko National University of Kyiv,* [2]*Institute of Physics, National Academy of Sciences, Ukraine*

selectivity of plasma-chemical transformations, providing high-enough productivity and efficiency of conversion at a relatively low electric power consumption on the high-voltage discharging in a flow at atmospheric pressure.

The non-equilibrium plasma assists as an energetic catalyst containing charged particles and electronically excited atoms and radicals, which initiate fast chain-branching conversion of hydrocarbons that does not occur in usual conditions. The highly developed plasma-liquid interface with the large surface-to-volume ratio and the deep injection of active plasma particles into the liquid also favor to the intensification of conversion in the plasma-liquid system. At that, there is no problem with excess heat removal since such plasma system is thermally "cold". The main idea is that the discharge can burn directly in the liquid fuel without preliminary gasification. In this part we report new results of the experimental and theoretical studies of the process of plasma-assisted reforming of ethanol in the PLS with the DC and pulsed DGCLW and TORNADO-LE using available methods of diagnostics and numerical modeling.

In the present work the results of experimental and theoretical investigation of plasma kinetics in new plasma chemical reactor are discussed. This device uses the reverse vortex gas flow of "tornado" type similar to Fridman's group (Fridman, 2008). Discharge of such type operates in the transitional thermal to non-thermal plasma regime. It is characterized by a presence of electrons with average electron energy of few electron volts and a neutral gas temperature of $\sim$ 1000-2000 K. High gas temperature increases hydrogen production as a result of the additional conversion of hydrocarbons generated in the discharge region. The presence of active O, OH and H in the mixture converts efficiently the hydrocarbons in the post-discharge region. The use of vortex air flow increases the stability of the discharge. An advantage of the proposed reactor over the one at (Prieto, 2001, Wang, 2004) is the use of a special working chamber. This chamber allows conversion of hydrocarbons either in the liquid or in the gas phase. In case of liquid, part of the input power goes into evaporation. The presence of liquid isolates the metallic electrode from the plasma region. It also prevents the electrode erosion and increases the working time of the reactor. The use of pyrolytic chamber allowed getting the energy efficiency value more than three times higher that such value for the similar plasma-liquid systems without pyrolytic chamber.

2. Equipment

Among possible types of electric discharges, which can produce non-thermal reacting plasma at high pressures, two specific cases are of research interest of scientists from Physic Electronics Department at the Taras Shevchenko National University of Kyiv. One source is the transverse arc in a blowing flow (BTA) that is an intermediate case of a high-voltage low-current self-sustained discharge with arc length adjusted by the transverse gas flow (Buchnev, 2000). It differs from the non-stationary gliding arc of Czernichowski type by the fixed arc length. It also has a convective cooling of the plasma by gas flow without conductive heat losses at the walls since it is a free arc jet. An intensive transverse gas ventilation of the BTA plasma increases its ionization nonequilibrium and non-isothermality (Chernyak, 2005). This factor has fundamental importance for plasma-chemical efficiency. Whereas the most of the discharge energy goes into the mean energy of electrons and not just to thermal heating, it gives desirable reactivity and selectivity of chemical transformations. BTA was tested successfully in the Kyiv University in different variants

with the primary and secondary discharges for the plasma processing of various homo- and heterophase gas and liquid substances, including plasma-assisted fuel combustion (Yukhymenko, 2007). Another potential source of non-thermal plasma that can provide simultaneously a high level of non-equilibrium and high density of reacting species in the plasma-liquid system is the electric discharge in a flowing gas channel with liquid wall (DGCLW). Its main properties are (Chernyak, 2008):

i. large ratio of the surface of plasma-liquid contact to the plasma volume;
ii. possibility of controlling of plasma-created gas-phase and hetero-phase components, which specifies its potential opportunities during plasma-liquid processing;
iii. possibility of using non-classic liquids including colloidal solutions and mash (waste liquids with fine solid aggregates);
iv. possibility to realize both DC and AC modes of discharge (in contrast with quasi-stationary modes of diaphragm discharges and capillary discharges).

DGCLW has been initially realized and investigated in plasma treatment of organics in air-water, phenol and toluene systems]. For the purposes of fuel reforming, DGCLW has been proposed in the KNU for the first time at the end of 2006. The idea is that DGCLW can be burning directly within the liquid hydrocarbon fuels without preliminary gasification (Chernyak, 2007).

The following setups were prepared with the PLS reactors with the DGCLW working with one and two gas streams injected into the homogeneous work liquid as is shown in Fig.1a and Fig.1b. It consists of the cooper rod electrodes (*1*), plasma column (*2*), work liquid (*3*), electrode in liquid (*4*), and quarts tubes (*5*). The discharge channel in the work liquid was formed in two ways: with a constant gas flow and without it. As a work gas, the standard technical air of atmospheric pressure is used. Ethanol, water, and ethanol-water mixtures were used as work liquids. Various modes of the discharge operation were tested:

i. the mode where the voltage applied to the electrodes mounted into the lower and upper flanges and the discharge was initiated between them;
ii. the mode where "+" was applied to the electrode mounted into the lower flange, whereas "–" was applied to the liquid ("liquid" cathode);
iii. the mode where "–" was applied to the electrode mounted into the lower flange, while "+" was applied to the liquid ("liquid" anode).

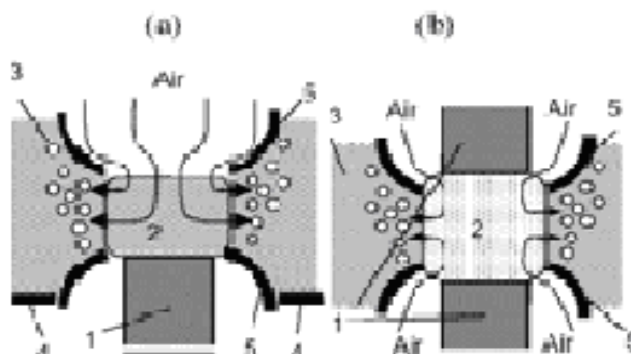Fig. 2 shows the dc DGCLW working in the mode I in water.

Fig. 1. Photo of discharge of air flow in water mode I with two solid electrodes.
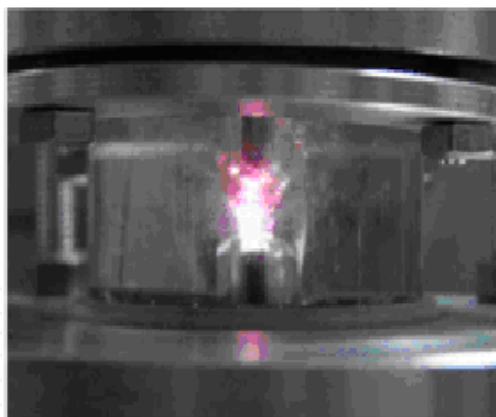
Fig. 2. Photo of discharge of air flow in water. Mode I with two solid electrodes.

Another PLS reactor was prepared with the DGCLW working with the air flow in the liquid under the induced microporous inhomogeneous conditions as is shown in Fig. 3. Here, the airflow was injected into the work liquid (*3*) through a copper tube (*1*) covered by a glass insulator (*2*) and it ran over a flat dielectric surface of the magnetostrictive transmitter (*5*) which produced ultrasonic cavitations, so the discharge channel (*4*) was formed by the air flow and water vapours (microbubbles). A high-voltage potential of ~4 kV was supplied between the gas input tube (*1*) and work liquid (*3*). The ultrasonic transmitter worked at the frequency of 18 kHz with the power ~ 20 W. Different modes of the discharge operation with the "liquid" cathode were tested:

i.   with airflow and ultrasonic;
ii.   with airflow and without ultrasonic;
iii. with ultrasonic and without airflow;
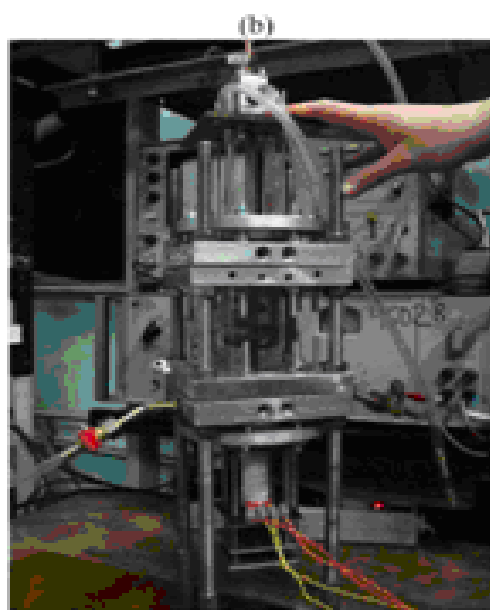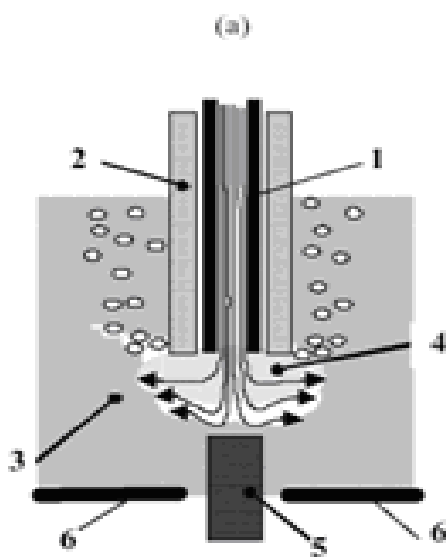iv.   and without airflow and ultrasonic.

Fig. 3. DCGLW (dc) in the liquid with microbubbles induced by ultrasonic cavitation. (**a**) - Scheme of discharge with liquid electrode; (**b**) – photo of pulsed reformer.

In addition to direct plasma reforming, also pyrolysis of ethanol after initial plasma-assisted reforming was studied by using the unit shown in Fig.4. The installation consists of two main parts: 1) plasma reactor, which treats ethanol-water mixture in the pulsed DGCLW, and 2) pyrolytic reactor, which treats ethanol-air vapors mixed with products generated by plasma reactor, where (*1*) is the Teflon insulator around the steel pins, (*2*) are steel pins through which voltage is applied, (*3*) are copper electrodes, conical bottom and top cylinder, (*4*) is a discharge plasma zone between electrodes, (*5*) is a vortex zone in the discharge, (*6*) is a bubbling zone in the liquid, (*7*) is the work liquid (solution of 96% pure ethanol and distilled water), (*8*) are mixing inlet and outlet chambers, (*9*) is the steel pyrolytic chamber; (*10*) are electric heaters, (*11*) is the cylindrical casing; (*12*) are thermocouples for temperature control, (*13*) is the glass vessel (0.5 l) for the output syngas collection.
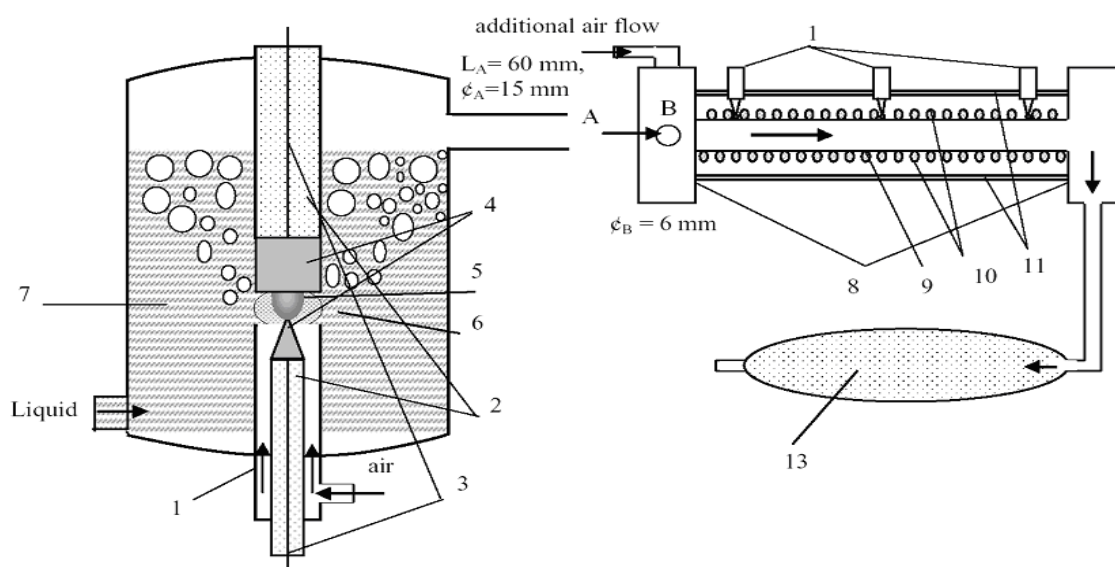

Fig. 4. Scheme of ethanol pyrolisis after plasma-assited reforming of ethanol-water mixture.

3. Diagnostic methods

Diagnostics of the DGCLW plasma was prepared by means of optical emission and absorption spectroscopy. The scheme of optical measurements is shown in Fig. 5.
Here, (*1*) is a quartz cylinder of the reactor, (*2*) are duralumin flanges, (*3*) are cooper electrodes, (*4*) are glass tubes for air input; (*5*) is a plasma column, (*6*) is the work liquid, (*7*) is a water cooling system, (*8*) is an input tube for work liquid, (*9*) is an output tube for gas products, (*10*) is a tube for the maintenance of constant pressure inside the reactor and communicating vessels, (*11*) is a spectral lamp source. A high-speed CCD-based spectrometer "Plasmaspec" with a spectral resolution ~0.6 nm is used for the spectra registration in the range of wavelengths 200-1100 nm. According to spectral measurements, the emission spectra of the DGCLW plasma in the air-water system are multi-component (Fig. 6) and contain character atomic lines H (656.3; 486.1; 434.0 nm) and Cu (electrode material) (324.7; 327.4; 465.1; 510.5; 515.3; 521.8; 578.2 nm), molecular bands of the 2+-system of N_2 ($C^3\Pi_u$-$B^3\Pi_g$), UV system of OH ($A^2\Sigma$-$X^2\Pi$, (0-0): 306.4-308.9 nm), also NH band ($A^3\Pi^+$-$X^3\Sigma^-$) and NO γ-system ($A^2\Sigma^+$-$X^2\Pi$).
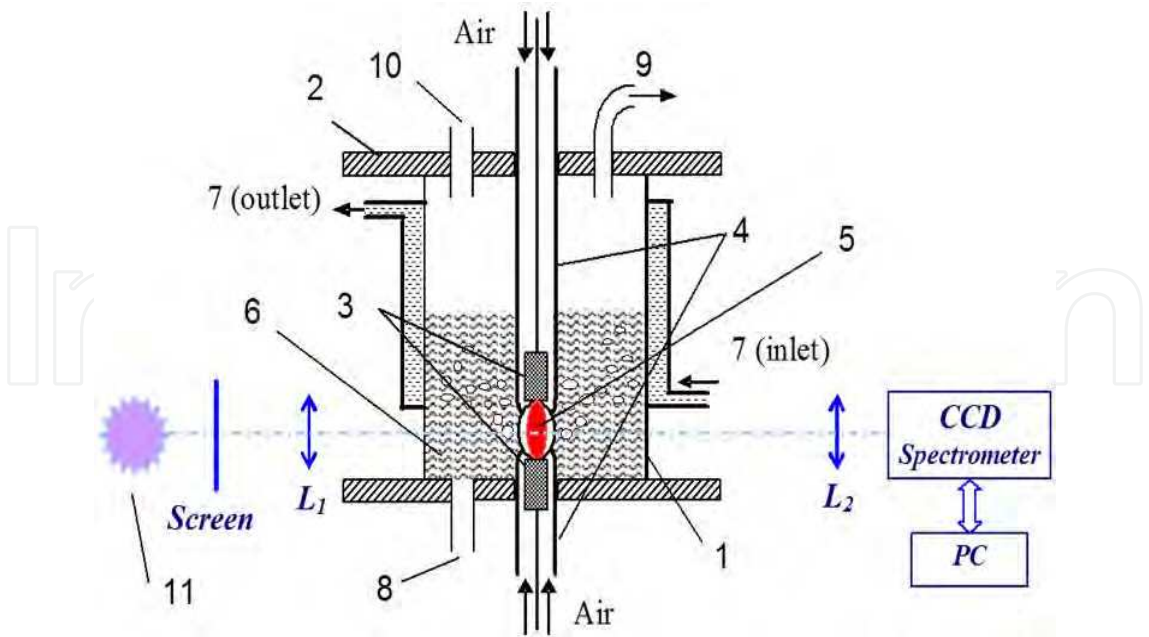
Fig. 5. Scheme of optical spectroscopy diagnostics of discharge plasma in the DGCLW.

The characteristic temperatures corresponding to excited states of atoms (electronic temperature T_e^*), and molecules (vibrational T_v^* and rotational T_r^* temperatures) in discharge plasma were determined by different methods. The electronic temperature T_e^* was determined by relative intensities of hydrogen emission lines H_α (656.3 nm) and H_β (486.1 nm) because these lines did no overlap with other spectral lines and bands. H_γ peak (434.0 nm) was not used because of its low intensity. Emission spectra of H lines were simulated by using a developed code Spec-Elements.

Fig. 6. Typical emission spectrum of air-water discharge plasma in the DCGLW.

This code allows calculations of absolute intensities of emission lines of elements (N, Ar, Cu, Fe, Ni, Co, Cr, etc) with using spectroscopic constants from the database of the Spectrum

Analyzer program (Navratil, 2006) and taking into account the instrumental function of the spectrometer. To determine T_e^* both experimental and simulated spectra were normalized on the H_α peak. In this case the height of H_β peak will directly depend on the T_e^* value.

The electronic temperature T_e^* was determined also by relative intensities of emission of oxygen multiplet lines (777.2; 844.6; 926.6 nm). To increase the accuracy of T_e^* determining it is necessary to chose spectral lines corresponding to electronic transitions from the energy levels with the maximal energy discrepancies of upper excited states E_2. Among OI lines observed in spectra the best pair is OI 777.2 nm (E_2=10.74eV) and OI 926.6 nm (E_2=12.08eV). Emission spectra of OI lines were simulated by using the SPECAIR program (SPECAIR, 2011). The dependence of the ratio of relative intensities of OI multiplet lines on the T_e^* values was plotted as a calibration curve. The spectral sensitivity of the used spectrometer was taken into account during the obtaining of corresponding intensities from experimental spectra. To determine vibrational T_v^* and rotational T_r^* temperatures, an original technique with using the SPECAIR program was developed. Since the emission of the OH ($A^2\Sigma$-$X^2\Pi$) bands is very intensive and its spectral structure is well characterized, it is a good monitor of T_r^* in plasma (Levin, 1999). It is a well-known method to use the *P*- and *R*- branches intensity ratio in the OH (0-0) band at wavelengths λ=306.4-308.9 nm for determination of T_r^* in plasma [16]. Because the peak of the *P*-branch is more self-absorbed than the peak of the *R*-branch, the *P/R* intensity ratio at given T_r^* becomes smaller as the optical thickness of plasma increases. A smaller *P/R* ratio would suggest T_r^* higher than its actual value. To avoid mistakes related with reabsorption it was proposed to use low intensive OH bands for determining T_r^*. A technique based on the SPECAIR simulation of the OH (1-0) and (2-1) bands, which are free from reabsorption, was suggested (Pryshiazhnevich, 2009).

Emission spectra were measured by the CCD spectrometer "Plasmaspec" as described before. The absolute intensities of calculated spectrum $I_{cal}(A_i)$ by using the SPECAIR at the fixed wavelengths (where the corresponding experimental signals $I_{exp}(A_i)$ were estimated) were determined. Then, the ratio of concentrations of radiating species A and B was evaluated by following formula:

$$\frac{[A_1]}{[A_2]} = \frac{I_{exp}(A_1) \cdot I_{cal}(A_2)}{I_{exp}(A_2) \cdot I_{cal}(A_1)}, \tag{1}$$

This makes possible to determine the relative concentration of each component in the investigated discharge plasma:

$$[A_1]^* = \frac{[A_1]}{\sum_i [A_i]} \tag{2}$$

Diagnostics by mass-spectrometry using a monopole mass-spectrometer MX 7301 and by gas-phase chromatography using a gas chromatograph 6890 N Agilent with the calibrated thermal conductivity detectors were prepared for the analysis of component content of the output gas products after the processing in the plasma-chemical reactor.

The typical mass spectrum of output gas products registered after the processing of ethanol-water mixture is shown in Fig. 7. The character components related to the mass ratios M/e = 2 (H_2^+), 12 (C^+), 14 (N^+), 16 (O^+, CH_4^+), 18 (H_2O^+), 28 (CO^+, N_2^+), and 32 (O_2^+) have been recognized.
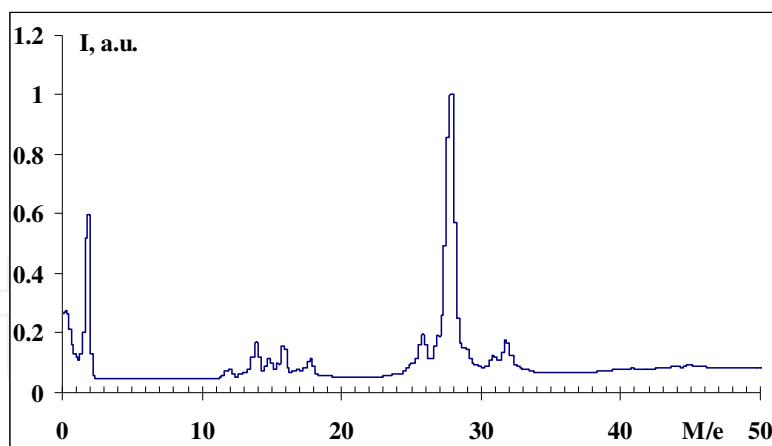
Fig. 7. Typical mass-spectrum of output gas products after the plasma reforming of ethanol - water mixture in the PLS with the DGCLW with the liquid cathode. I_d=300 mA, G= 55 cm^3/s.

4. Numerical models

The physical model of DGCLW-PLS was based on the next assumptions:
-   electric power introduced in the discharge is immediately averaged in the discharge volume;
-   internal electric field in the discharge does not vary in space and time;
-   during the pass of air through the discharge into the reactor volume its content is totally refreshed and its flow rate in the reactor volume is the same as in the discharge gap.

The mathematical modelling of DGCLW-PLS was developed with the next features:
-   calculation of the electron energy distribution function on the base of solution of the Boltzmann equation in two-term approximation (Raizer, 1997);
-   hydrodynamic modeling in quasi-1D fluid volume averaged approximation (Shchedrin, 2008).
-   kinetic modeling by solution of the system of chemical kinetic equations for kinetically valuable components of air-ethanol-water plasma system (Shchedrin, 2011).

The kinetic mechanism includes 59 components (C_2H_5OH, N_2, O_2, CO, etc), 76 electron-molecular processes and 364 chemical reactions with a set of corresponding cross sections and rate constants compiled according to update NIST kinetic databases (NIST, 2011).

As a case study, the comparative analysis of the developed method of simulation of kinetic processes in the plasma-liquid system in the electrical discharge in the gas channel with liquid wall and other known methods of calculations of plasma kinetics in micro-discharges was conducted. It was shown that the averaging of the energy that deposited into the discharge in the whole gas channel volume is the principal feature of the developed method.

4.1 Modeling of dusty plasmas with liquid microparticles
Complex (dusty) plasmas are gas plasmas consisting of electrons, ions, and neutral atoms that additionally contain microscopic particles with sizes ranging from 10 nm to 10 μm. These micro-particles may be solid or liquid. It is well-known (Frenkel, 1975) that many features of these states are very similar. From this point of view will be useful produce a review of generalities of both types of microparticles and give a special account of

distinctive features of liquid substances. Essential differences of liquid particle from solid one mostly connected with special features of liquid surface. It is clear that addition of electric charge makes new peculiarities in this situation.

The main parameters of liquid drop are:

1. geometrical – what type of approximation is selected: ball-shaped (main factor is its radius) or spheroid (main factor is its eccentricity);
2. physical – mass/volume density; dielectric permittivity; surface tension coefficient; viscosity; specific conductivity; evaporation and coagulation;
3. chemical – composition; existence of surface-active substance (SAS).

The theoretical model should describe basic phenomena in dusty plasma. They are:

i. Elementary processes in dusty plasma;
ii. Dynamical processes in dusty plasma;
iii. Waves and instabilities in dusty plasmas.

Some quality conclusions can be made:

1. The droplet surface is unstable, because thermal capillary waves are disturbed.
2. The maximal surface charge (Q_{max}) exists.
3. This charge (Q_{max}) is the reason of drop decay. The method of this problem solving arises from Bohr – Frenkel theory of nuclear decay.
4. The decay path is a function of viscosity (γ) and dielectric permittivity (ε) = f(ε, γ). If liquid in drop has a conductivity and its viscosity is small, the drop will be disintegrated on some hundreds little droplets with radius a_i << R. If liquid in drop is dielectric, the drop has 2-particle decay. Their full charge is equal to initial Q and their radius a_i ≤ R.
5. Changes in chemical composition or SAS additions make the surface charge variability.
6. Interaction of charged drop with laminar air flow is resulted decay criterion lower.
7. Linear vibration of charged drop surface can produce the electromagnetic radiation.
8. Surface of uncharged drop (incompressible) can produce the acoustic wave in definite frequency range. Surface charging will intensify this effect. It can be used for diagnostics of liquid dusty particles in plasma of the DGCLW.

4.2 Kinetics: Modeling and calculations

A global model is used in our calculations, with an assumption that the discharge is homogeneous over the entire volume. It is justified at zero approximation, because the time of the gas mixing in radial direction is less than the times of characteristic chemical reactions. Also neglected is the processes in the transitive zone between the discharge to post-discharge. The volume of the transitional zone is much smaller than the volume of discharge and post-discharge zones. Thus, the time of gas pumping through the transition region is too short for the chemical reactions to have a sufficient influence on the concentration of neutral components.

The total time of calculation is divided into two time intervals: the first one is the calculation of the kinetic processes of fast generation of active atoms and radicals in the discharge region. Those components accelerate the formation of molecular hydrogen, carbon oxides and other hydrocarbons production. The second time interval is the oxidation of the gas mixture in the post-discharge region as a result of the high gas temperature and the presence of O and OH. These components remain in the mixture after the dissociation of water and oxygen molecules by electrons impacts in plasma. The oxidation of generated hydrocarbons (mainly C_xH_y and formaldehyde CH_2O) has noticeable influence on kinetics

in the investigated mixture due to high gas temperature (1000 K). Under aforementioned conditions, the characteristic time of oxidation is approximately equal to the air pumping time through the discharge region (10^{-3}-10^{-2} s). Therefore, the low temperature plasma model (Chernyak, 2008, Shchedrin, 2008), where the continuous discharge is divided into the sequence of quasi-constant discharges, is not applicable here. The following system of kinetic equations is used in order to account the constant air pumping through the system:

$$\frac{dN_i}{dt} = S_{ei} + \sum_j k_{ij} N_j + \sum_{j,l} k_{ijl} N_j N_l + ... + K_i - \frac{G}{V} N_i - k N_i \cdot \tag{3}$$

It is calculated using a solver developed at the Institute of Physics National Academy of Science, Ukraine was verified many times on other systems and has demonstrated good results. N_i, N_j, N_l in equation (3) are concentrations of molecules and radicals; k_{ij}, k_{iml} are rate constants of the processes for i-th component. The rates of electron-molecule reactions are:

$$S_{ei} = \frac{W}{V} \frac{1}{\varepsilon_{ei}} \frac{W_{ei}}{\sum_i W_{ei} + \sum_i W_i}, \tag{4}$$

where W is the discharge power and V is the discharge volume. In this model, W is the full power W_0 divided by factor of two. This division corresponds to the most stable regime of the discharge (Fridman, 2008). The value of W_0 is determined by the current-voltage characteristic. W_{ei} is the specific power deposited into the inelastic electron-molecular process with threshold energy ε_{ei}:

$$W_{ei} = \sqrt{\frac{2q}{m}} n_e N_i \varepsilon_{ei} \int_0^\infty \varepsilon Q_{ei}(\varepsilon) f(\varepsilon) d\varepsilon. \tag{5}$$

Here $q = 1.602 \cdot 10^{-12}$ erg/eV, m is the mass of electron and n_e is the concentration of electrons. The variable Q_{ei} is inelastic process cross section, $f(\varepsilon)$ is the electron energy distribution function (EEDF); W_i is the specific power deposited into elastic processes:

$$W_i = \frac{2m}{M_i} \sqrt{\frac{2q}{m}} n_e N_i \int_0^\infty \varepsilon^2 Q_i(\varepsilon) f(\varepsilon) d\varepsilon. \tag{6}$$

Here M_i are the molecules masses, Q_i are the transport cross sections for nitrogen, oxygen, water and ethanol molecules.
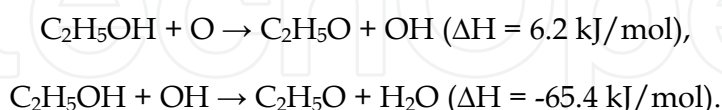
The last three terms in equation (3) describe the constant inflow and outflow of gas from the discharge region. The term K_i is the inflow of molecules of the primary components (nitrogen, oxygen, water and ethanol) into the plasma, $\frac{G}{V} N_i$ and $k N_i$ are the gas outflow as the result of the air pumping and the pressure difference between the discharge region and the atmosphere.

In order to define the initial conditions, the ethanol/water solution is assumed to be an ideal solution. Therefore, the vapors concentrations are linear functions of the ethanol-to-water ratio in the liquid. The evaporation rates K_i of C_2H_5OH and H_2O are calculated from the measured liquids consumption. The inflow rates K_i of nitrogen and oxygen are calculated by the rate of air pumping through the discharge region:

$$K_i = \frac{G}{V} N_i^0,$$ (7)

where N_i^0 correspond to $[N_2]$ and $[O_2]$ in the atmospheric pressure air flow.

In the non-equilibrium plasma almost the entire energy is deposited into the electron component. The active species, generated in the electron-molecular processes, lead to chain reactions with ethanol molecules. The released energy heats the gas. Calculations show that the fastest reactions of that type are:

$$C_2H_5OH + O \rightarrow C_2H_5O + OH \ (\Delta H = 6.2 \ kJ/mol),$$

$$C_2H_5OH + OH \rightarrow C_2H_5O + H_2O \ (\Delta H = -65.4 \ kJ/mol).$$

The first reaction is endothermic and the second is exothermic. By comparing their specific enthalpies, one can estimate the average gas temperature, which is near 1200 K. The gas temperature in the discharge region is taken to be constant in the model. In reality the gas temperature T is dependent on the gas pumping rate and the heat exchange with the environment. Therefore, in order to account of those influences, T is varied in the interval 800-1500 K (similarly to experimentally obtained temperature spread).

After ~10^{-2} s the balance between the generation and the decomposition of the components leads to saturation of concentrations of all species. It allows to stop the calculations in the discharge region and to investigate the kinetics in the post-discharge region. The system (1) is solved without accounting of the last three terms on the time interval without plasma. The calculations are terminated when the molecular oxygen concentration reaches zero level. That time interval equals to a few milliseconds. The gas temperature in this region is found using the equation (Kosarev, 2008):

$$\frac{dT}{dt} = -\frac{1}{\rho C_p} \sum_i H_i(T) \cdot \mu_i \frac{dN_i}{dt}.$$ (8)

Here ρ is the gas density, C_p is the average specific gas heat capacity under constant pressure, H_i and μ_i are molar enthalpy and molar mass of i-th component respectively.

It is seen from equations (5-6) the specific powers W_{ei} and W_i are influenced by the electron energy distribution function. EEDF is calculated from Boltzman kinetic equation in the two-term approximation for breakdown field in the air (Soloshenko, 2007). The last assumption was made due to the fact that nitrogen is a plasma-forming gas. Only the processes with the primary components (see table 1) are taken into account in EEDF calculations. The cross sections of processes 17-19 are absent in the recent literature. Therefore, in order to estimate these cross sections, an approximation (Soloshenko, 2007) was used. At this approximation the cross section of ethanol is equal to the cross section of oxygen biased on the doubled threshold energy.

Fig.8 shows the calculated EEDFs for different gas temperatures and 6.5% ethanol concentration in solution. It is shown that EEDF is defined by vibrations of water molecules (two levels ((100)+(010)) and (010)), excited by electrons, whose energy is less than 0.05 eV. In the 1.5-2 eV region EEDF is defined by the excitation of electron-vibrational levels of nitrogen and water by electron impact. When the electrons' energy is higher than 8 eV EEDF looks like Maxwell distribution function. At this region the function's behavior is defined by

the dissociation and ionization of molecules by electrons' impacts. The average electrons' energy is 0.55 eV for 800 K, 0.46 eV for 1200 K and 0.43 eV for 1500 K.

№	Reaction
1.1	$H_2O + e \rightarrow H_2O((100)+(010)) + e$
2.1	$H_2O + e \rightarrow H_2O(010) + e$
3.1	$H_2O + e \rightarrow OH + H + e$
4.1	$H_2O + e \rightarrow H_2O^+ + 2e$
5.1	$H_2O + e \rightarrow H_2O(J = 0\text{-}0) + e$
6.1	$H_2O + e \rightarrow H_2O(J = 0\text{-}1) + e$
7.1	$H_2O + e \rightarrow H_2O(J = 0\text{-}2) + e$
8.1	$H_2O + e \rightarrow H_2O(J = 0\text{-}3) + e$
9.1	$N_2 + e \rightarrow N_2(A^3\Sigma_u^+) + e$
10.1	$N_2 + e \rightarrow N_2(a^1\Pi_g) + e$
11.1	$N_2 + e \rightarrow N_2(v) + e$
12.1	$N_2 + e \rightarrow N + N + e$
13.1	$N_2 + e \rightarrow N_2^+ + 2e$
14.1	$O_2 + e \rightarrow O + O + e$
15.1	$O_2 + e \rightarrow O_2(^1\Delta_g) + e$
16.1	$O_2 + e \rightarrow O_2^+ + 2e$
17.1	$C_2H_5OH + e \rightarrow CH_3 + CH_2OH + e$
18.1	$C_2H_5OH + e \rightarrow C_2H_5 + OH + e$
19.1	$C_2H_5OH + e \rightarrow CH_3CHOH + H + e$
20.1	$C_2H_5OH + e \rightarrow C_2H_5OH^+ + 2e$

Table 1. Reactions which were taken into account in the EEDF calculations

There is no generally accepted kinetic mechanism for modeling plasma kinetics in air/water/ethanol mixture. In the previous works (Chernyak, 2008, Shchedrin, 2009), a mechanism for the low temperature region was proposed.

However, this mechanism does not describe kinetics in "tornado" type electrical discharge, where the gas temperature is much higher. Main mechanism (Marinov, 1999) and ethanol sub-mechanism (Dagaout, 2008) could be more appropriate for describing the chemical reactions in the investigated mixture. The preliminary calculations have shown that these schemes include many unneeded components which do not contribute to the end product in the investigated regimes. They may be ignored in the scheme of reactions. Dunphy proposed a kinetic mechanism for high-temperature ethanol oxidation in (Dunphy, 1991). The investigated temperature interval (1080-1660 K) in that article is close to the one at present work. Therefore, Dunphy's scheme was chosen as the basic mechanism in the research. It was expanded by Held's methanol sub-mechanism (Held, 1998) and by additional important processes in hydrogen oxidation (Konnov, 2008): $OH+OH+M \rightarrow H_2O_2+M$, $OH+OH \rightarrow H_2O+O$, $H+H+M \rightarrow H_2+M$, $H_2+O_2 \rightarrow OH+OH$, $H_2+O_2 \rightarrow H+HO_2$. The full mechanism developed in this work is presented in table 2. It is composed of 30 components and 130 chemical reactions between them. The charged particles (electrons and ions) were ignored in the mechanism, because of low degree of ionization of the gas (~10^{-6}-10^{-5}). Nitrogen acts as the third body in the recombination and thermal dissociation reactions. Additionally, the nitrogen-containing species were removed from the mechanism,

since they are not the subject of this study. Also, the research (Levko, 2010) has shown that the processes between these components and hydrocarbons were third-order reactions.
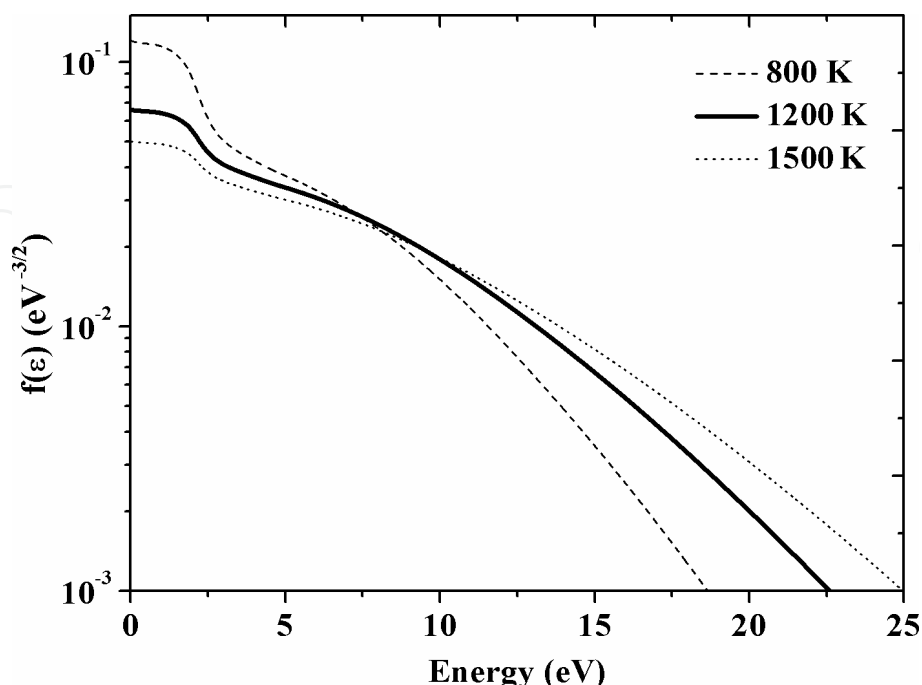

Fig. 8. Calculated electron energy distribution functions at 6.5% ethanol concentration in the liquid.

4. Results and discussion

The applicability of the developed methods for diagnostics of the discharge plasma parameters was tested in the DGCLW in different modes of operation: with two solid electrodes or with one liquid electrode of different polarity, i.e., liquid anode or liquid cathode.

Typical operating parameters in nominal regime were following: discharge current I_d= 200 mA, voltage U= 1.6 kV, airflow rate G= 55 cm^3/s. Emission spectra of investigated plasma were registered by the CCD spectrometer "Plasmaspec" in the range of wavelengths λ= 200-1100 nm.

For estimation of electronic excitation temperatures T_e^* in plasma, the relative intensities of atomic emission lines of Cu (λ= 465.1; 510.5; 515.3; 521.8; 578.2 nm) and H (λ= 486.1, 656.6 nm) were analyzed. As a result, a set of characteristic electronic temperatures T_e^*(H) = 4300 K and T_e^*(Cu) = 7200 K was obtained for the investigated regime of the discharge operation.

For estimation of vibrational and rotational excitation temperatures T_v^* and T_r^* in plasma, the relative intensities of molecular emissions of the OH (A-X) bands (1-0) at 283.1 nm and (2-1) at 288.4 nm and the N$_2$ (C-B) bands (0-2) at 380.1 nm and (1-3) at 375.1 nm were analyzed on the base of the SPECAIR simulation. Results of the fitting of experimental and simulation spectra in the selected spectral intervals are shown in Fig. 9.

The best fit in Fig.9 was found for the following set of temperatures: T_v^*(OH) = 3800K, T_r^*(OH) = 3200K, T_v^*(N$_2$) = 4000K, T_r^*(N$_2$) = 2000K. The discrepancy between measured and calculated spectra in Fig. 9a in contrast to Fig. 9b can be explained by the fact that the

simulation of the OH (A-X) emission was made without taking into account the N_2 (C-B) emission that occurs in the same spectral region.
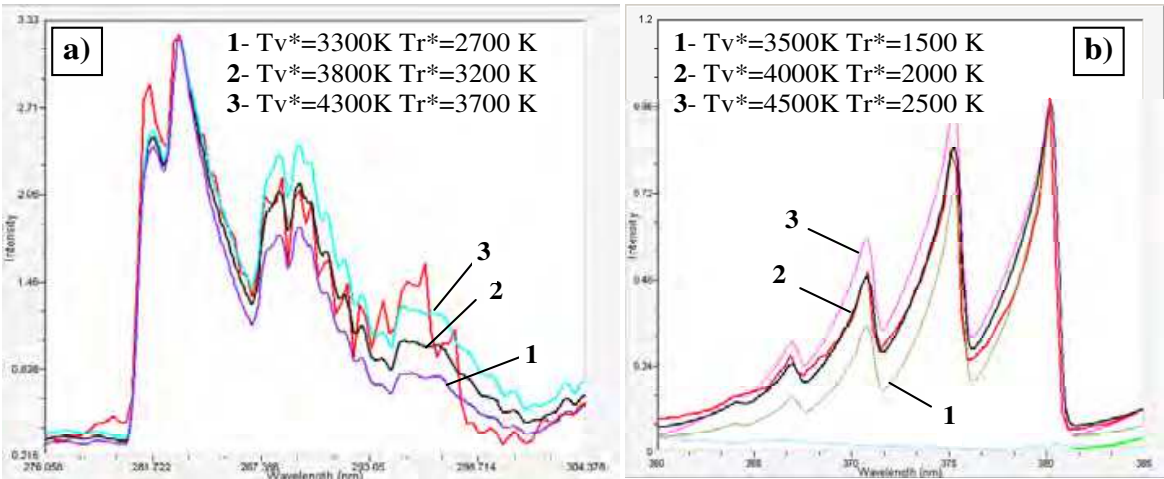

Fig. 9. SPECAIR simulation (curves 1, 2, 3) and experimental (red curve) spectra of the DGCLW in water: (**a**) OH (A-X) bands at 275-304 nm; (**b**) N_2 (C-B) bands at 360-385 nm.
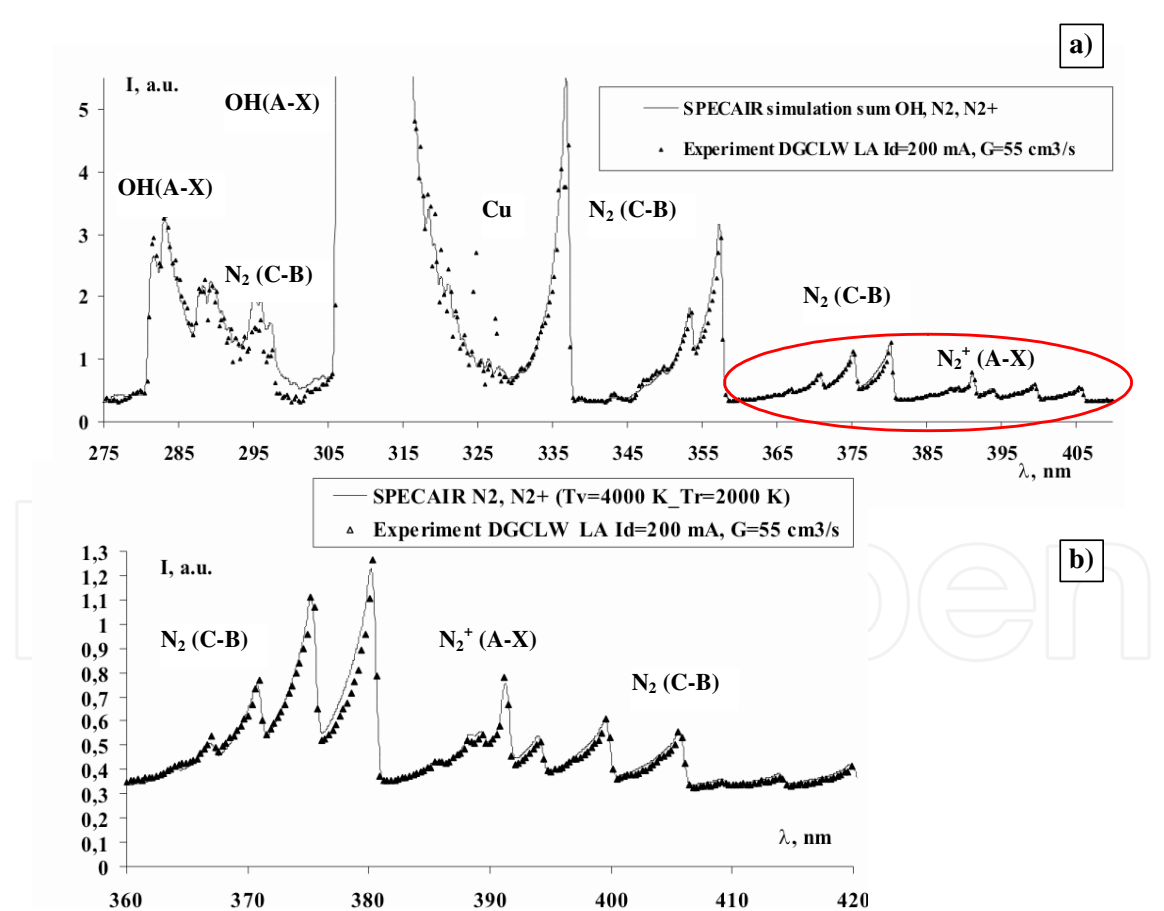

Fig. 10. SPECAIR simulation and experimental spectra of the DGCLW in water: (**a**) emission in the range 275-405 nm; (**b**) magnified spectral range 360-420 nm in the red oval. Characteristic temperatures: T_v^*(OH)=3800 K, T_r^*(OH)=3200 K, T_v^*(N_2, N_2^+)=4000 K, T_r^* (N_2, N_2^+)=2000 K.

Fig. 11. Absorption spectra (left) of water solution after the plasma treatment in the DGCLW for different processing times (curves 1-7 are from 15 to 600 s) and dependences (right) of UV absorption at 380 nm on the exposure time in the discharge with (grey curve) and without ultrasonic cavitations (black curve).

Applying the absorption spectrophotometry, the absorption spectra of work liquids after the plasma treatment in the DGCLW-PLS reactor with and without ultrasonic cavitations were measured. According to data obtained (Fig. 11), the absorption spectra of the treated liquid consist of UV absorption bands of ions of nitrous acid HNO_2. Its spectral distribution does not change very much with and without US treatment, but the intensity of the absorption band at 350 nm permanently grows with the exposure time (Fig. 10.a). It means that the concentration of the HNO_2 products in the treated liquid grows proportionally to the time of the plasma treatment, and this process proceeds more intensively under the influence of the ultrasonic cavitations (Fig. 11b).

Analyzing the emission spectra in plasma of the pulsed DGCLW working in different modes with and without ultrasonic field, the dependences of relative intensities of molecular OH (A-X) and N_2 (C-B) bands and atomic H_α, H_β lines were obtained. Also, using the ratio of H_α and H_β lines, the temperature of the population of H electronic states $T_e^*(H)$ was estimated.

It was found that the ultrasonic field differently affects the behavior of various components of plasma emission in the DGCLW. The relative intensity of OH (A-X) emission non-monotonic increases with increasing exposure time, but it quickly reduces under the ultrasonic cavitations. Relative intensity of N_2 (C-B) emission is almost independent on exposure time with and without ultrasonic field.

Relative intensity of H_α emission linearly increases with increasing exposure time in both modes with and without ultrasonic; however, the ultrasonic field reduces the rate of this growth for half time. Despite the growth of the relative H_α emission intensity, the electronic temperatures $T_e^*(H)$ are virtually the same, i.e. the ultrasonic field has no visual effect on the behavior of T_e^*.

It is important to note that all components of emission spectra observed have lower relative emission intensities in the presence of the ultrasonic field. This can be explained that the ultrasonic at 17 kHz may be easily transmitted in air. Moreover, the features of the plasma-liquid surface interaction at the boundary between the phases can favor to the penetration of the ultrasonic field into the gas phase. Then, the ultrasonic cavitations in plasma can increase the probability of the quenching of excited states of atoms due to enhanced

collisions. As a result, total intensity of radiation in plasma may decrease with the time under the ultrasonic field.

The distributions of character temperatures T_e^*, T_r^*, T_v^* in plasma in the DGCLW working in water at air flow rate G=55cm^3/s at currents I_d=50-400 A for three different modes: with solid electrodes, with solid cathode + liquid and with liquid cathode + solid anode were investigated. Electronic temperatures T_e^*(H) and T_e^*(Cu) were determined by using relative intensities of atomic lines H_α, H_β (656.5, 486.1 nm) and Cu I (465.1, 510.5, 515.5, 521.8, 578.2 nm). The vibrational and rotational temperatures, T_v^* and T_r^* were determined by using relative intensities of molecular bands N_2 (C-B) (0-2) at 380.1 nm and (1-3) at 375.1 nm and OH (A-X) (1-0) at 283.1 nm and (2-1) at 288.4 nm.

In common, the temperatures T_e^*(Cu) in the DGCLW with the liquid electrode gradually increase with increasing discharge current, however, for the mode of liquid anode the T_e^*(Cu) are considerably larger than for the mode of liquid cathode. This difference in the values of character temperatures in the discharge modes with the liquid electrodes is also observed for all other plasma components with the exception of T_e^*(H). With the liquid cathode the T_e^*(H) noticeable increases, whereas with the liquid anode the T_e^*(H) slightly decreases. Larger values for character temperatures in plasma of the DGCLW with the liquid cathode for almost all components (except Cu) may be explained by greater energy input in discharge plasma. For T_e^*(Cu), its larger value for the liquid anode follows by the decrease of the absolute intensity of Cu emission lines (if compared with other two modes); this may indicate a reduction in output of Cu from the electrodes in this regime.

Analyzing the obtained values and dependences, one can conclude that the investigated DGCLW generates non-equilibrium reacting plasma whose parameters are close to non-equilibrium plasma of the gliding arc, which is effectively used in non-thermal atmospheric-pressure plasma-assisted initiation and plasma-supported combustion of hydrocarbon fuels (Fridman, 2008). The results of OES diagnostics of plasma in the DGCLW working in pure ethanol and ethanol/water mixture (5/1) at the air flow rate G=55cm^3/s at currents I_d=50-400 A in the mode with two solid electrodes are shown in Fig. 11.

From the temperature dependencies in Fig. 12 one can reveal that the transition from the water to the pure ethanol in the DGCLW does not affect very much character temperatures T_e^*(Cu), T_e^*(H) and T_r (OH), except CN, when noticeable difference between T_r and T_v takes place. The last fact demonstrates the effect of thermalization and reduction of non-equilibrium in plasma. Possible reason may be additional energy input from ethanol due to initiation of combustion processes in the plasma-fuel system.

The results of OES diagnostics of plasma in the DGCLW working in the mode with the liquid anode in ethanol/water mixture (5/1) at the air flow rate G=55cm^3/s at currents I_d=50-400 A are shown in Fig. 12. From the temperature dependences obtained one can reviled that in the investigated regimes in the DGCLW working with the liquid anode, the characteristic temperatures for radical CN are close T_v (CN) ≈ T_r (CN) and for molecule C_2 are differ T_v (C_2) > T_r (C_2). At that, T_v (CN) and T_r (CN) exceed T_v (C_2) a little bit (~20%). With increasing discharge current from 100 mA to 400 mA, all temperatures are decreased from 4000-5000 K to 3000-4000 K.

Fig. 14. shows the fragments of emission spectra related to the C_2 ($d^3\Pi_g$-$a^3\Pi_u$) Swan band emission in the spectral range 516-570 nm as obtained in plasma of the DGCLW with the liquid cathode working in ethanol/water mixture (5/1) with and without US field. One can see that fragments are almost identical, so the effect is practically absent. It can be explained

by the possible depletion of ultrasonic cavitations in the work liquid caused by additional gas evolution in plasma-liquid system due to reforming.
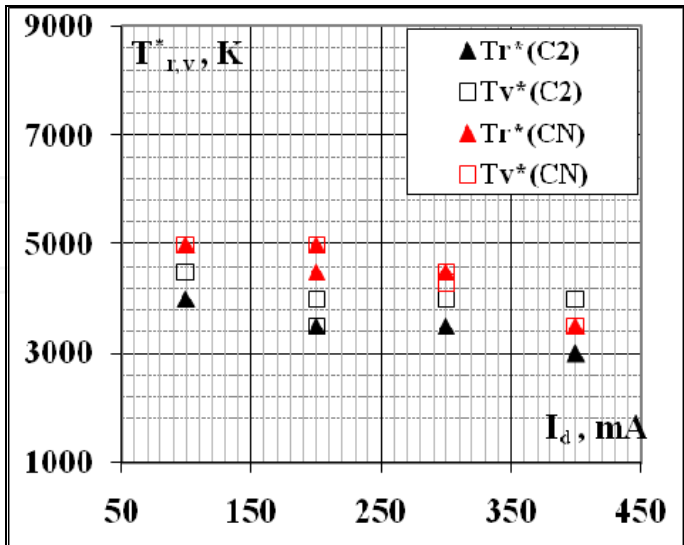

Fig. 12. Character temperatures T_r, T_v in discharge plasma vs. current in the DGCLW with the liquid anode working in ethanol/water mixture (5/1). Air flow rate G=55 cm³/s.
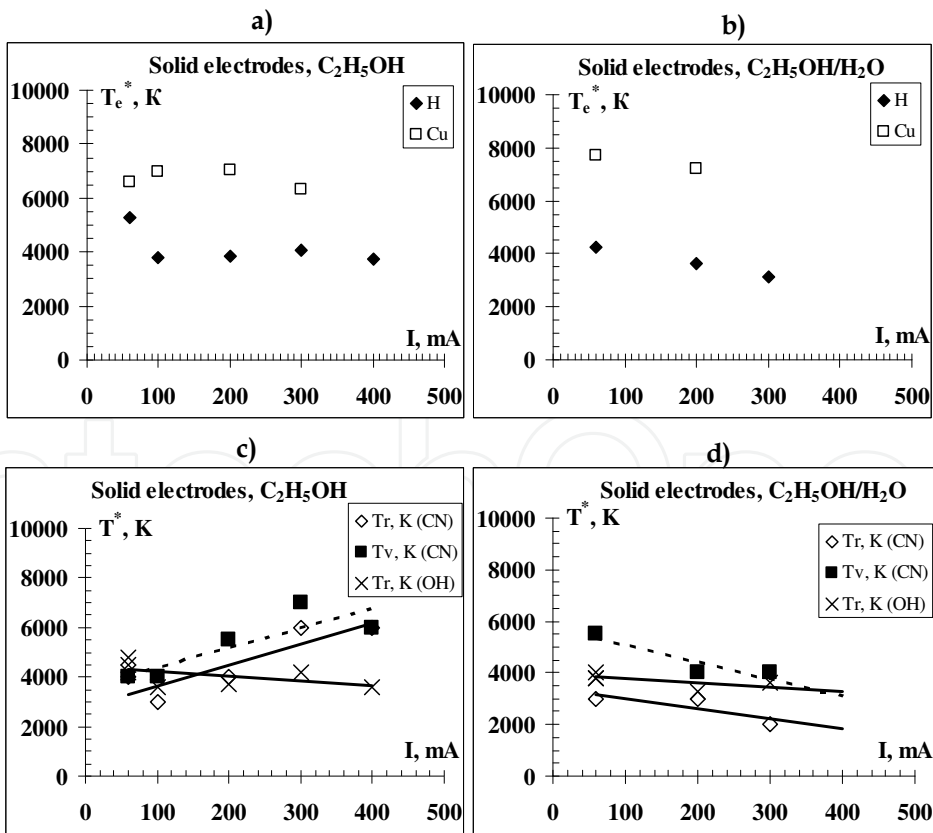

Fig. 13. Character temperatures T_e^*, T_r^*, T_v^* in discharge plasma vs. current in the DGCLW with solid electrodes: (a, c) are pure ethanol, (b, d) are ethanol/water mixture (5/1). Air flow rate G=55 cm³/s.

Fig. 14. Spectral distribution of the C_2 ($d^3\Pi_g$-$a^3\Pi_u$) emission in plasma of the DC DGCLW with liquid cathode working in ethanol/water mixture (5/1) with and without US field. Discharge current I_d = 100 mA, air flow rate G=55 cm^3/s.

The current-voltage and power characteristics of the DC DGCLW working in ethanol-water solution are shown in Fig. 15. A dropping character of *I-V* curves at discharge currents from 100 to 400 mA indicates the transition regime from the abnormal glow to the arc discharge.

Fig. 15. Current-voltage (left) and power (right) characteristics of the DGCLW working in different modes in ethanol-water solution (5/1). Air flow rate G= 55 cm^3/s.

The results of mass-spectroscopic and gas-chromatographic measurements of concentrations of basic components in output gas products after the ethanol processing in the DGCLW at different discharge currents are shown in Figs. 16-17. These data are given for the case of mixture $C_2H_5OH : H_2O$ = 5:1 and airflow rate G=55 cm^3/s.

Fig.19 shows the results of numerical modeling and calculations of concentrations of H_2, CO_2 and other main stable components in output gas products after the ethanol processing in the PLS with the DGCLW. The qualitative and quantitative agreement between calculated and measured data is quite good, at least, for main components. One can see that the output concentration [H_2] grows linearly with the discharge current and it reduces exponentially with the gas flow rate.

In the discharge conditions, the kinetics of the H_2 formation is determined mainly by the reaction $C_2H_5OH + H \rightarrow CH_3CH_2O + H_2$. Since the ethanol concentration [C_2H_5OH] in solution changes slowly, the [H_2] production is determined entirely by the concentration of
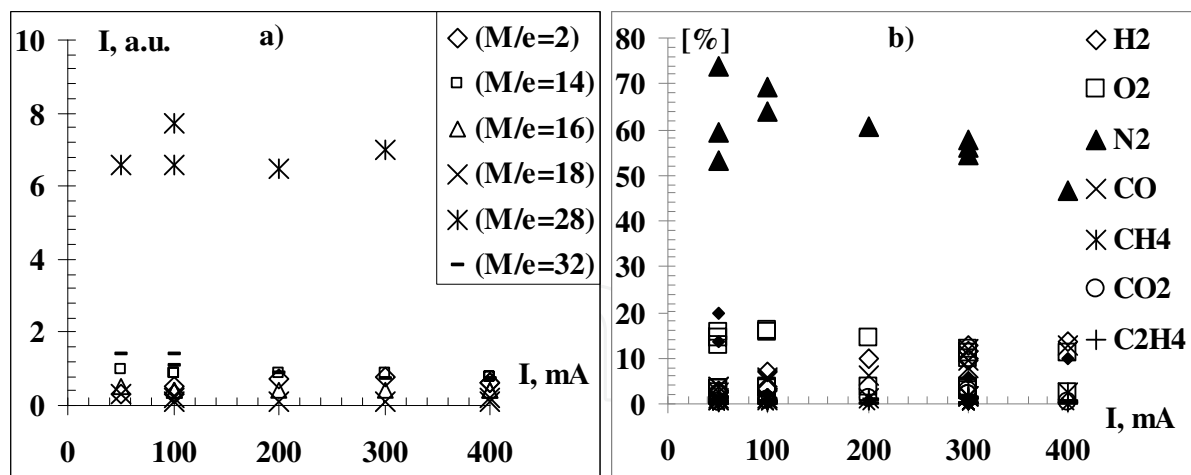
Fig. 16. Data of mass-spectrometry (a) and gas-chromatography (b) analysis of output gas products after the ethanol processing in the DGCLW. The mass ratio M/e = 2 is H_2^+, 12 is C^+, 14 is N^+, 16 is O^+, $CH4^+$, 18 is H_2O^+, 28 is CO^+, N_2^+, and 32 is O_2^+.
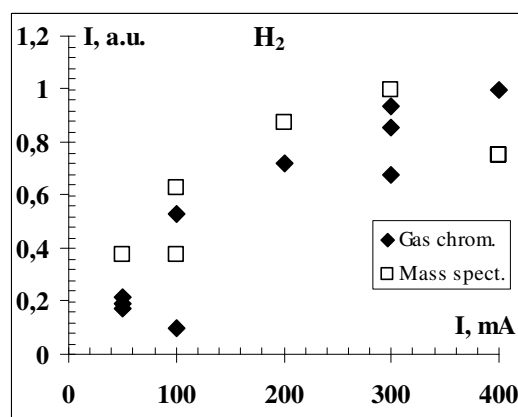

Fig. 17. Content of H_2 in output gas products after the ethanol processing in the DGCLW. Ethanol-water solution (5/1), airflow rate G=55 cm³/s.
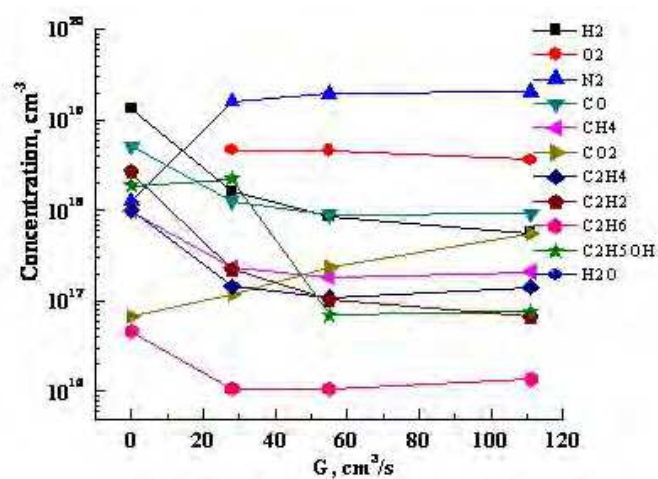

Fig. 18. Concentrations of output gas products after the ethanol processing in the DGCLW as function of air flow rate. Ethanol-water solution (5/1), I_d= 100 mA.

Fig. 19. Calculated concentrations of output gas products after the ethanol processing in the DGCLW as functions of discharge current (left, G= 55 cm³/s) and air flow rate (right, I_d= 100 mA). $C_2H_5OH : H_2O = 5:1$.

atomic hydrogen [H]. In the case under consideration, the main process responsible for the generation of H is the dissociation of water molecules H_2O by the direct electron impact. The rate of this process is proportional to the specific electric power deposited to discharge (i.e., discharge current). Therefore, the [H_2] production is also a linear function of the discharge current in accordance with experimental data. Outside the discharge, the only process that influences the H_2 concentration is the water-gas shift reaction $CO + H_2O \rightarrow H_2 + CO_2$. Via this process, the system reaches the complete conversion of CO into CO_2 and H_2.

The estimation of efficiency of the proposed method of the plasma reforming of liquid ethanol into synthesis gas in the PLS-DGCLW reformer was performed on the basis of thermo-chemical calculations using criteria: (a) energy cost of 1 m³ syngas products; (b) productivity of conversion; (c) specific heat of 1 m³ syngas combustion, and (d) energy efficiency.

Calculations were made with taking into account standard thermo-chemical constants of hydrocarbons (NIST, 2011) using the coefficient of energy transformation (Chernyak, 2007):

$$\alpha = \frac{\sum_i Y_i \times LHV\,(Y_i)}{IPE}, \tag{9}$$

and also for the conversion efficiency by (Petitpas, 2007):

$$\eta = \frac{(Y_{H2} + Y_{CO}) \times LHV\,(H_2)}{IPE + Y_{HC} \times LHV\,(HC)} \tag{10}$$

Here, IPE is the input plasma energy, Y is the molar fraction, LHV is the lower heating value of syngas components, HC is the hydrocarbon fuel (ethanol). The formula (4) assumes that CO can be totally transformed into H_2 by the water-gas shift reaction with zero energy cost.

The results of estimations in the form of α (I) and η (I) dependencies for the ethanol reforming in the DGCLW for different discharge modes against the discharge power are presented in Fig.20.
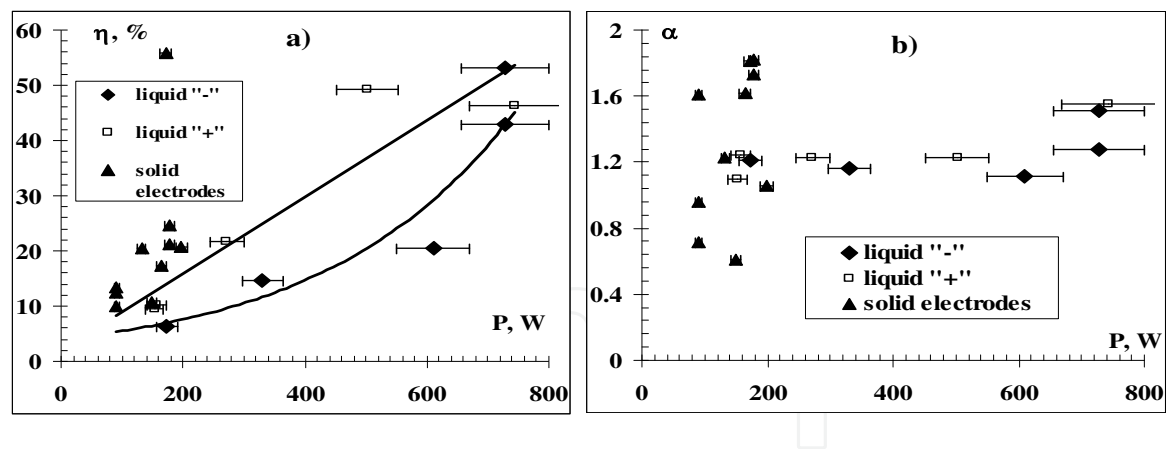
Fig. 20. Dependencies of (a) efficiency of conversion η and (b) coefficient of energy transformation α for the ethanol reforming in the DGCLW in different discharge modes as a function of the discharge power (currents vary from 50 to 400 mA). $C_2H_5OH : H_2O = 5:1$

Fig. 21 shows the values of coefficient a and parameter η together with data of mass-spectrometry of H_2 in the DGCLW for different modes at different discharge currents. One can see that that the coefficient α for the mode of solid electrodes has the same growth trend with increasing current as the H_2 yield. And for modes of liquid electrode the parameter of efficiency η has the same trend of growth as the H_2 yield. This difference in behavior of parameters may be caused due to the fact that the power of discharge using the liquid electrode is proportional to the current. At smaller currents the efficiency is of 20%, at large currents the efficiency is at 45-55%. For the modes of liquid electrode with increased current the level of efficiency of reforming is higher than for the mode of solid electrodes. At that, each mode demonstrates increased efficiency with increasing current.
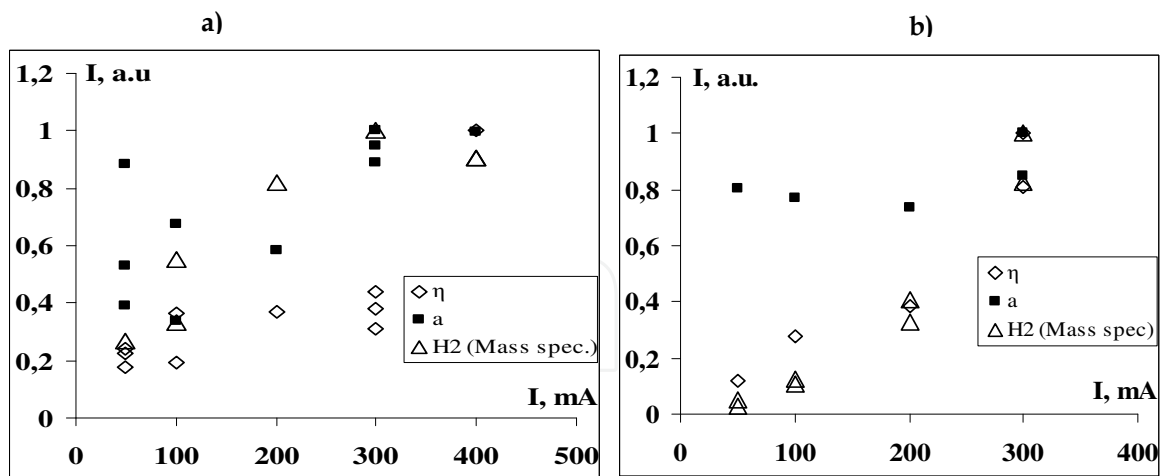

Fig. 21. Coefficient of energy transformation α, conversion efficiency η and H_2 yield as measured by mass-spectrometry for the ethanol reforming in the DGCLW at different currents: a) mode of solid electrodes; b) mode of liquid cathode.

One can see that the net H_2 yield in the discharge at $I = 300$ mA is ~15% whereas the energy efficiency of the ethanol conversion into the syngas is up to 50%. (input energy is 4-10% of $LHV = 26.8$ MJ/kg).These numbers correlate with the earlier results (Chernyak, 2008) and are comparable with other known plasma-aided ethanol reforming methods (Petitpas, 2007).

The impact of the plasma-forming gas on the ethanol reforming in the DGCLW was also studied. For that, the composition of gas-phase products of conversion in the reactor and the coefficient of energy transformation were studied at different gas flow rates. Research was conducted for the mode of solid electrodes. The composition and mixture ratio under the ethanol reforming were taken the same as in previous research. The discharge current varied between 100 and 400 mA, the air flow rate varied from 0 to 110 cm^3/s.

Fig. 22. shows the results for I= 100 mA that demonstrates a good matching between gas chromatography and mass-spectrometry data. For other currents the same matching is observed. It should be noted that with increasing air supply in the discharge the concentration of H_2 in syngas products decreases. In fact, the highest yield of H_2 is observed in the discharge mode without air supply. But the time of H_2 production in this case increases considerably, and the power consumption also increases. All this reduces the coefficient of energy transformation (Fig. 22). Moreover, this decreases the lifetime of the system. Therefore, the total system performance without air supply seems to be not very good.
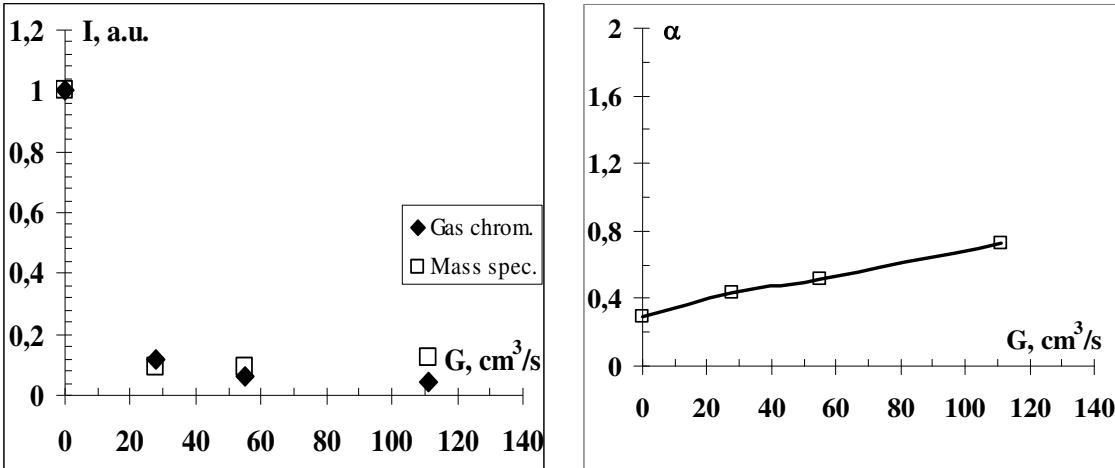

Fig. 22. Coefficient of energy transformation α for the ethanol reforming in the DGCLW with solid electrodes at different air flow rates. I_d =100 mA.

The results of the studies of the post-discharge pyrolysis of ethanol after initial plasma-assisted ethanol reforming are presented in Figs.23-24. The experimental parameters were following: discharge frequency 420 Hz, air flow rate 17-28 cm^3/s, time of treatment up to 10 min (600 s); the temperature in the pyrolytic chamber varied from 0 to 870 K. The principal feature of the pulsed discharge power supply in comparison with dc mode is the ability to work with higher energy input in plasma at comparable power capacity. This gives more intensive plasma stimulation of pyrolysis due to deep injection of plasma in the pyrolytic chamber.

Fig.24. shows the H_2 as measured by mass-spectrometry and partial H_2 content in syngas as measured by gas-chromatography after the ethanol pyrolysis in a pyrolytic chamber. One can see a good correlation between GC and MS data. Also noticeable that the H_2 production in the pyrolytic chamber without discharge is very low (indicated by empty signs).

Fig. 25 shows the coefficient of energy transformation α for the reforming system as a function of temperature in the pyrolytic chamber. It is seen that values α increase with increasing temperature. Some modes with the change of air flow (modes 5+2 and 5+3

correspond to additional air supply into the pyrolytic chamber comparably with the air supply in the discharge) have lower energy efficiency than the mode with the constant air flow because of variation of partial output of isobutane C_4H_{10}. Fig. 45 shows the rate of syngas production in the reforming system. One can conclude that the investigated combination of electric discharge + post-discharge pyrolysis for the ethanol reforming demonstrates the smart efficiency of this approach.
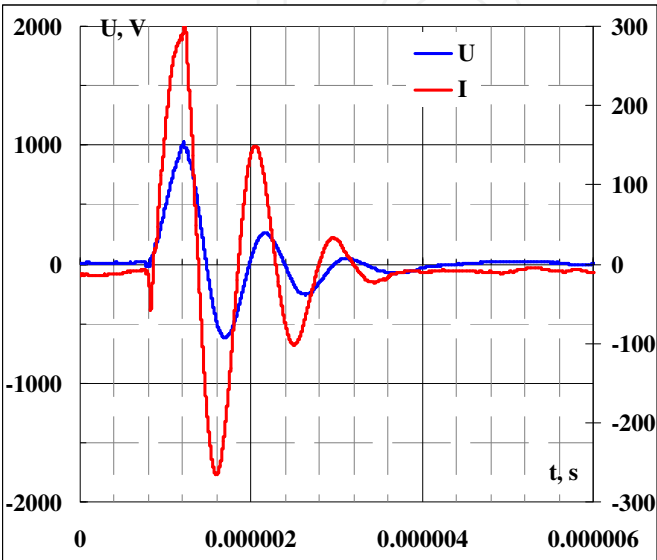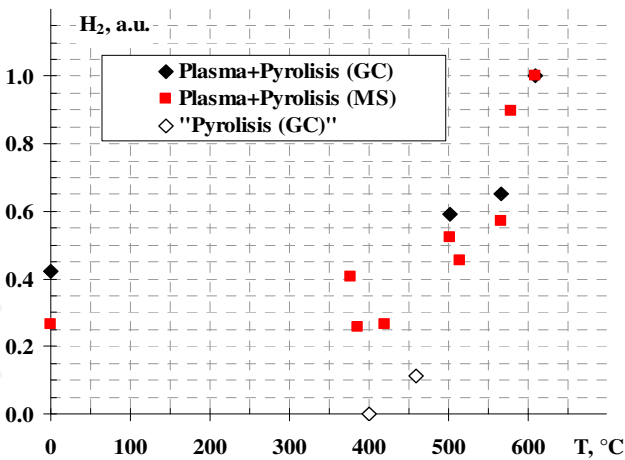
Fig. 23. Voltage and current oscillograms in the pulsed DGCLW.

Fig. 24. H_2 as measured by mass-spectrometry and partial H_2 content in syngas as measured by gas chromatography after the ethanol pyrolysis vs. temperature in the pyrolytic chamber.

5.1 TORNADO-LE: Experimental results

As it is mentioned above, various methods using thermal and non-thermal plasma for fuel reforming are known. Thermal plasma, which is thermodynamically equilibrium, has characteristics of high ionization by higher energetic density. This has merits of good rate of fuel decomposition but demerits of poor chemical selectivity and high specific energy
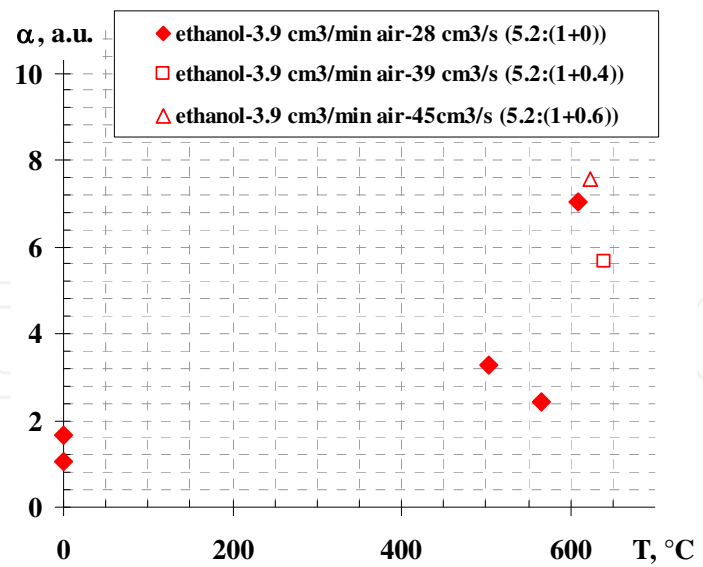
Fig. 25. Coefficient of energy transformation *a* vs. temperature in the pyrolytic chamber.
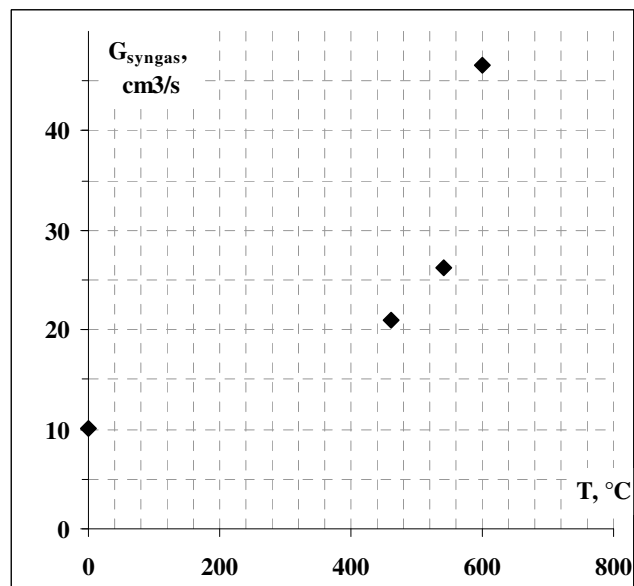

Fig. 26. The rate of syngas production vs. temperature in the pyrolytic chamber.

consumption. Non-thermal (low-temperature) plasma, which is kinetically non-equilibrium, has characteristics of low ionization but benefits of high reactivity and selectivity of chemical transformations providing high enough productivity at relatively low energy consumption; this can be obtained by high voltage discharge in a flow at low or high atmospheric pressures. or reforming with plasma support (pyrolysis, steam reforming, partial oxidization) it is preferable to utilize the high plasma flow rate generators: the pulsed systems and systems on the base of TORNADO discharge type (Chernyak, 2010).

PLS reactor with the DC discharge in a reverse vortex gas flow of Tornado type with the "liquid" electrode (TORNADO-LE) as is shown in Fig.27 has been prepared. It consists of a cylindrical quartz vessel (1) by diameter of 9 cm and height of 5 cm, sealed by the flanges at the top (2) and at the bottom (3). The vessel was filled by the work liquid (4) through the

inlet pipe (5) and the level of liquid was controlled by the spray pump. The basic cylindrical T-shaped stainless steel water-cooled electrode (6) on the lower flange (3) made from stainless steel is fully immersed in the liquid. The electrode on the upper flange (2) made from duralumin had a special copper hub (11) with the axial nozzle (7) by diameter 2 mm and length of 6 mm. The gas was injected into the vessel through the orifice (8) in the upper flange (2) tangentially to the cylinder wall (l) and created a reverse vortex flow of tornado type, so the rotating gas (9) went down to the liquid surface and moved to the central axis where flowed out through the nozzle (7) in the form of jet (10) into the quartz chamber (12). Since the area of minimal static pressure above the liquid surface during the vortex gas flow is located near the central axis, it creates the column of liquid at the gas-liquid interface in the form of the cone with the height of ~1 cm above the liquid surface (without electric discharge).
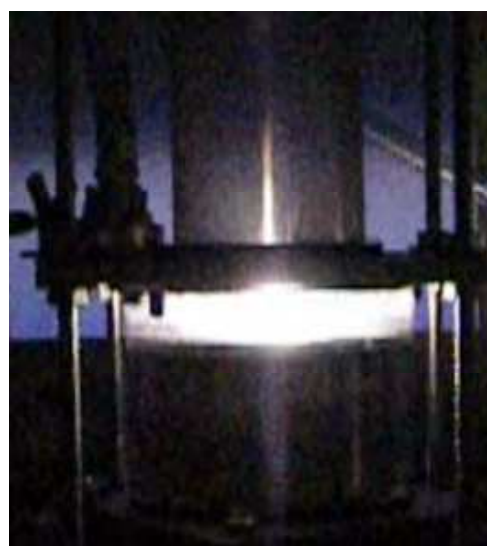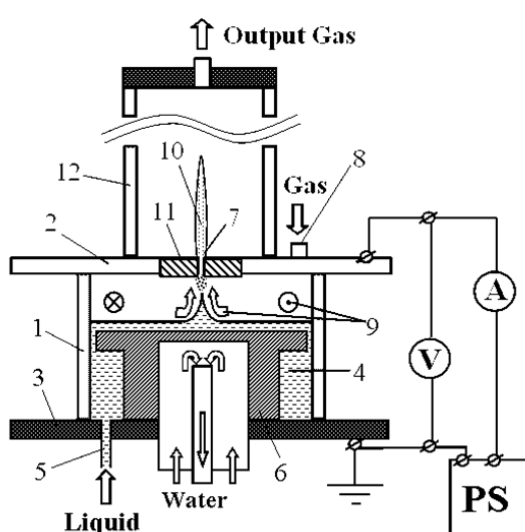

Fig. 27. Schematic (left) of the PLS reactor with the DC discharge in a reverse vortex gas flow of Tornado type with a "liquid" electrode and photo (right) of the TORNADO-LE working in ethanol-water solution.

The voltage was supplied between the upper electrode (2) and the lower electrode (6) in the liquid with the help of the DC power source powered up to 10 kV. Two modes of the discharge operation were studied: the mode with "liquid" cathode (LC) and the mode with "liquid" anode (LA): "+" is on the flange (2) in the LC mode, and "-" is on the flange (2) in the LA mode. The conditions of breakdown in the discharge chamber were regulated by three parameters: by the level of the work liquid; by the gas flow rate G; and by the value of voltage U. The ignition of discharge usually began from the appearance of the axial streamer; the time of establishment of the self-sustained mode of operation was ~1-2 s. The range of discharge currents varied within 100-400 mA. The pressure in the discharge chamber during the discharge operation was ~1.2 atm, the static pressure outside the reactor was ~1 atm. The elongated ~5 cm plasma torch (10) was formed during the discharge burning in the camera.

The typical current-voltage characteristics of the TORNADO-LE with the liquid anode working in water at different airflow rates are shown in Fig. 28.

Typical emission spectra of plasma in TORNADO-LE inside and outside of reactor are shown in Fig.29. All this spectra were normalize on maximum at wavelength λ_n =306,7 nm.

Hydroxyl OH and nitrogen N_2 bands, hydrogen H_α (656.3 nm), H_β (486.1 nm), copper Cu and oxygen multiplet O (777.2; 844.6; 926.6 nm) lines are on emission spectra. Nitrogen band N_2(C-B) and copper lines Cu was presented only outside of system.
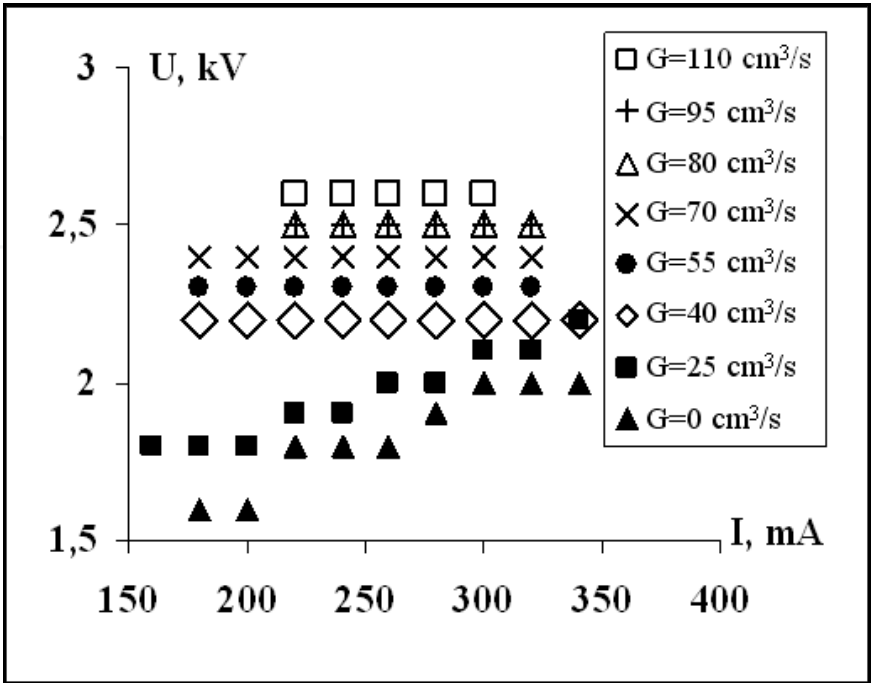

Fig. 28. Current-voltage characteristics of TORNADO-LE with the liquid anode working in ethanol-water solution at diffrent airflow rates.
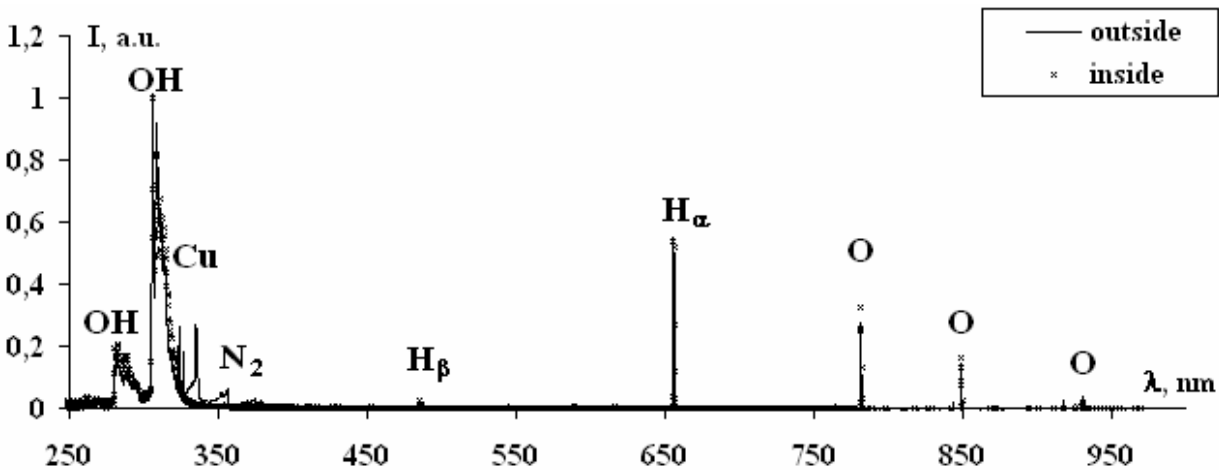

Fig. 29. Typical emission spectrum of discharge plasma inside and outside of reactor in the TORNADO-LE: I=300 mA; G=55 cm^3/s; U=2,3 kV; working liquid – distilled water; gas flow – air; mode with solid cathode.

Emission spectra in PLS TORNADO-LE working on distilled water measured at different discharge currents are shown in Fig.30. The electronic temperature T_e^* was determined by relative intensities of hydrogen emission lines H_α (656.3 nm), H_β (486.1 nm), relative intensities of emission of oxygen multiplet lines (777.2; 844.6; 926.6 nm)

Excitation temperatures for regime I = 300 mA, G=55 cm^3/s, U=2,3 kV in the mode SC were measured. Excitation temperatures inside of reactor was T_r^*=4000±500 K, T_v^*=4000±500 K and T_e^* = 5000±500 K. Plasma temperatures outside of reactor was T_r^*=4500±500 K, T_e^*=3000±500 K and T_v^*=5000±500 K. Excitation temperatures vibrational T_v^* and rotational T_r^* was obtained by band of OH. Plasma in PLS TORNADO-LE inside of reactor was isothermal. But outside of reactor plasma was non-isothermal.

Experimental and calculated emission spectra by the SPECAIR are shown in Fig. 31. Results of mass-spectrometry of output syngas products after the ethanol reforming in the TORNADO-LE are shown in Fig.32. One can see that content of H_2 and CO in output syngas products is quite high.
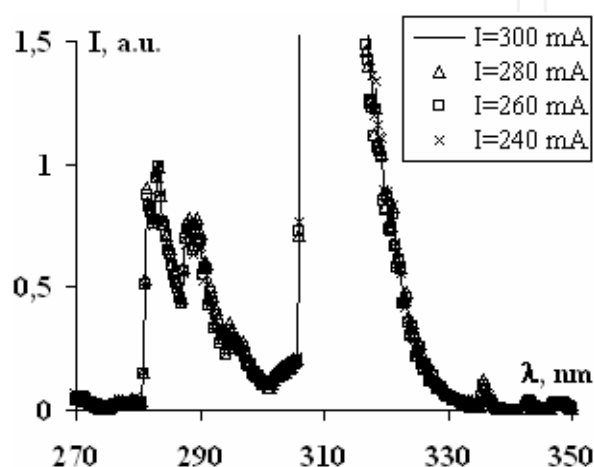

Fig. 30. Emission spectra of discharge plasma in the TORNADO-LE inside of reactor at different discharge currents: working liquid – distilled water; mode with SC; air flow G=55 cm^3/s.
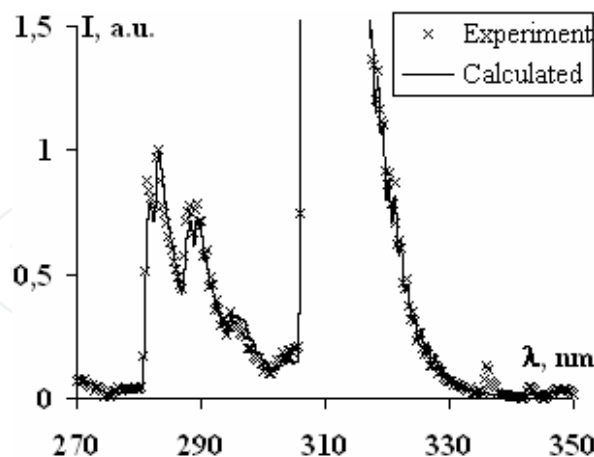

Fig. 31. Experimental emission spectrum of discharge plasma inside of system in the TORNADO-LE and calculated emission spectra by the SPECAIR.

The estimated coefficients of energy transformation (Petitpas, 2007) for the ethanol reforming in the PLS with the TORNADO-LE depending on the initial ethanol concentration in the ethanol-water mixture are presented in Fig.33. One can see that values α are quite high and reach ~0.8 at 25% ethanol-water solution.
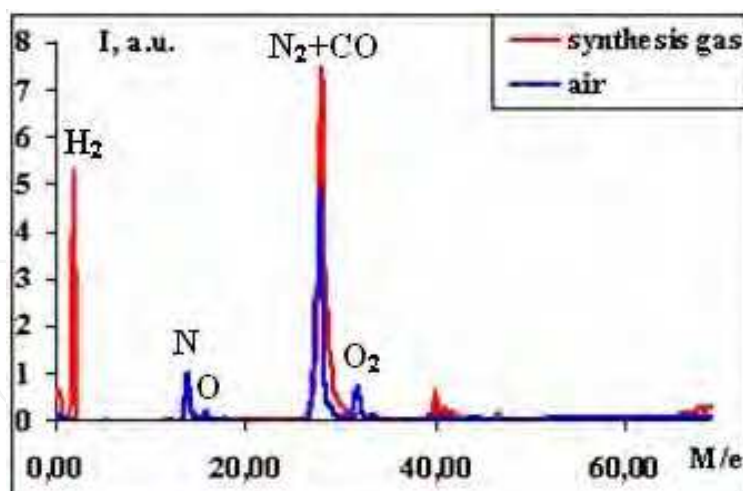
Fig. 32. Mass-spectrometry of gas products after the reforming in the TORNADO-LE with liquid cathode. Voltage 2 kV, current 320 mA, air flow rate 55 cm^3/s, mixture C_2H_5OH/H_2O = 1/4.
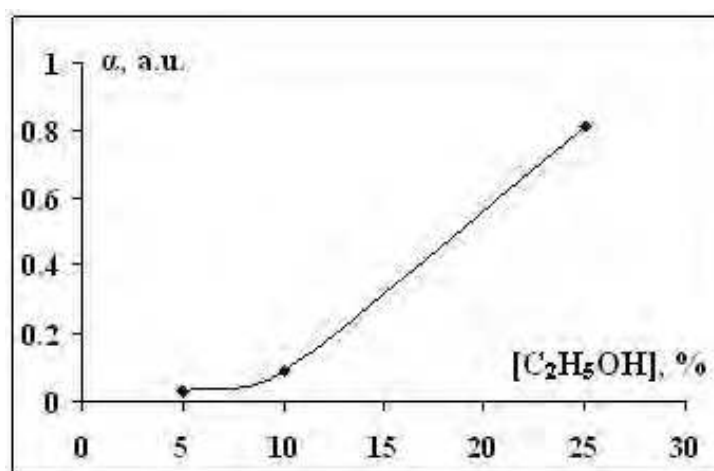

Fig. 33. Coefficient of energy transformation for the ethanol reforming in the TORNADO-LE as a function of the initial ethanol concentration.

5.1.1 TORNADO-LE: Experimental results

The composition of the gas at the output of the reactor is analyzed by the gas-phase chromatography using a gas chromatograph 6890 N Agilent with calibrated thermal conductivity detectors. The measurements show, that the main components of the mixture that leave the reactor are H_2, CO, CO_2, CH_4, C_2H_4, C_2H_6 and C_2H_2. This result is in good agreement with the results of numerical simulation. Fig.12 shows the comparison between experimental and computational data for different ethanol-to-water ratios in the solution. It is seen that the measured data are in a good agreement with computed ones. When ethanol concentration is 6.5% and 13% at T = 1500 K, then hydrogen and carbon monoxide are the main components of the gas mixture. Fig.34 shows the sum of concentrations of H_2 and CO, since CO converts fully into H_2 by water gas shift reaction (CO+H_2O → H_2+CO_2). This process was not taken into account in the kinetic mechanism, because its rate constant is too low to have sufficient influence on kinetics in discharge and post-discharge regions of the

subject reactor. The best agreement between measured and calculated data at 26% ethanol concentration is reached at T = 1000 K.
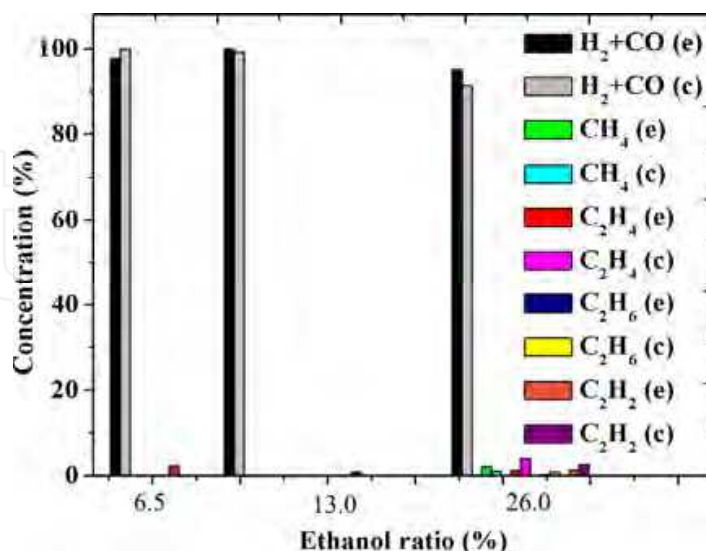

Fig. 34. Comparison between calculated (c) and experimentally (e) obtained concentrations of main components.

In order to define molecular hydrogen yield, the following expression is used (Petitpas, 2007):

$$Y(H_2) = \frac{[H_2]}{3 \cdot [C_2H_5OH] + [H_2O]}. \tag{10}$$

Here H_2 concentration is taken on the outlet of the reactor, and the values of ethanol and water concentrations are taken at the beginning of the discharge phase. Fig.35 shows the calculated dependences of hydrogen yield from gas temperature for different ethanol concentrations. It is seen that in all three cases the yield $Y(H_2)$ grows when T increases. Additionally, the highest yield is reached when ethanol concentration in the solution is 13% and T = 1500 K. Under these conditions H_2 generation process is efficient through the abstraction of hydrocarbons (7) and through the water H-abstraction (8).

Fig.36 presents the increase of H_2 yield at the post-discharge region as compared to the yield at the discharge region. It is seen that the use of the combustion zone is more beneficial in case of low ethanol concentration in liquid at high temperatures. On one hand, the increase of the ethanol-to-water ratio increases ethanol's flow rate (from 1 ml/min to 2 ml/min) and the initial ethanol vapor concentration. On the other hand, the growth of $[C_2H_5OH]$ leads to a decrease of both $[H_2O]$ and the rate of the channel (9). Fig. 36 shows, that the factor of water concentration decrease is much more dominant than the factor of ethanol concentration increase. Therefore, the highest molecular hydrogen yield is reached for 13% concentration of ethanol. These results are in good agreement with the results on Fig.35.

An important characteristic of plasma chemical reactor is its efficiency:

$$\eta = \frac{(Y_{H2} + Y_{CO}) \times LHV(H_2)}{IPE + Y_{HC} \times LHV(HC)} \tag{11}$$
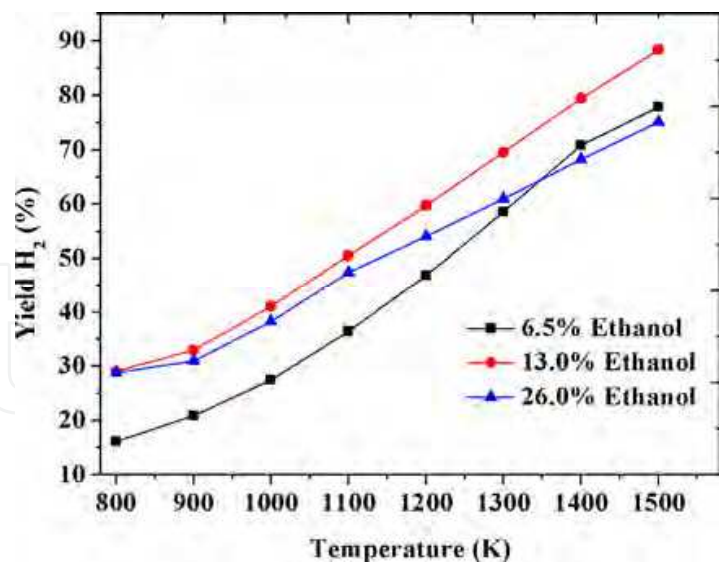
Fig. 35. The calculated dependence of the molecular hydrogen yield from the gas temperature.
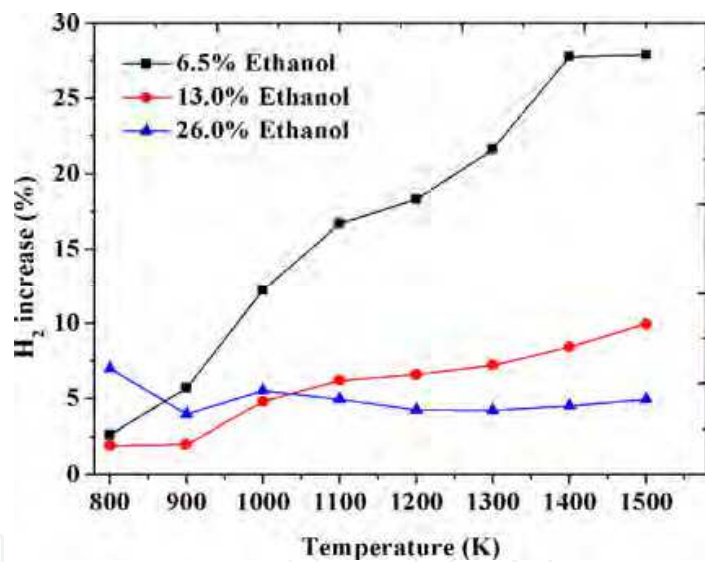

Fig. 36. The increase of yield of the molecular hydrogen as a result of the use post-discharge region

Here the sum of hydrogen and carbon oxide yields due to water gas shift reaction is taken. Also in (11) *LHV* is the lower heating value of the hydrogen and the fuel (ethanol), *IPE* is the introduced plasma energy. It is seen from Fig. 37 that the highest η value is 6.5% at ethanol concentration of 26%. It is much lower than the values obtained by the Massachusetts Institute of Technology and the Waseda University groups for pure ethanol (Bromberg, 2006). However, this reactor has a higher value of conversion rate than the named groups' reactors. This characteristic is calculated from the expression (Petitpas, 2007):

$$\chi = \frac{[CO + CO_2 + CH_4 + ...]_{produced}}{2 \cdot [C_2H_5OH]_{injected}}.$$ (12)

The last formula describes the efficiency of breaking C-C and C-H bonds in ethanol molecule. Fig. 38 shows that the highest χ is reached at 6.5% of [C_2H_5OH] in the solution. Such behavior is associated with the post-discharge region, where ethanol is fully oxidized. The reactions between the stable hydrocarbons and the active species do not change the sum in the numerator of (12). They lead to the redistribution of carbon atoms between carbon oxides and C_xH_y. Let us note that χ value, which can be larger than 100%, is attributed to the constant ethanol pumping through the discharge zone.
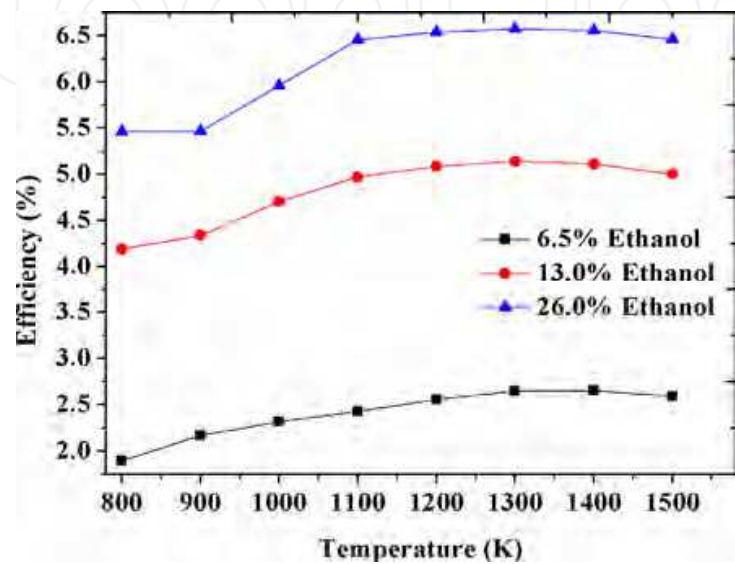

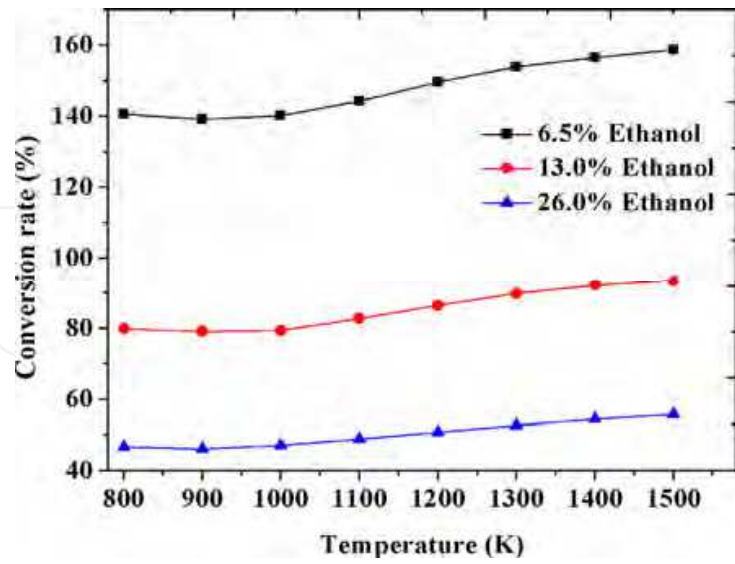Fig. 37. The efficiency of researched plasma chemical reactor for different mixtures

Fig. 38. Conversion rate of researched plasma chemical reactor for different mixtures

Thus, the results of the preliminary studies demonstrate that the glow discharge in the reverse vortex flow of Tornado type with the liquid electrode is very perspective for the plasma-assisted reforming of liquid hydrocarbon fuels.

6. Conclusions

It is shown that plasma in the investigated regimes is non-thermal: $T_e^*(Cu) > T_e^*(H) \geq T_v^*(N_2) \approx T_v^*(OH) \geq T_r^*(OH) > T_r^*(N_2)$. The observed discrepancy between electronic temperatures of Cu and H atoms is explained by the additional mechanism of population of the excited electronic states of Cu atoms due to the electron-ion recombination. The observed discrepancy between rotational temperatures determined by the OH (A-X) and N_2 (C-B) bands is not well understood and needs further careful examination.

The study of emission spectra of plasma in the blowing transverse arc discharge in a regime of the plasma-assisted fuel combustion in the system of utilization of syngas products after the plasma fuel reforming has shown the following:

• Significant differences in distributions of intensities of spectral atomic lines and molecular bands in the plasma plume along the flow depending on the fuel presence in the air flow. The addition of fuel in the mixture reduces the maxima in the distributions.

• Considerable influences on distributions of electronic temperatures T_e^* of atomic species (H, O) and vibrational T_v^* and rotational T_r^* temperatures of molecular species (N_2, OH, CN, C_2) in the plasma plume along the flow from both the electrode materials (Cu) and the components of air/fuel mixture (O, N, H). All of them correlate within the measurement uncertainty approximating by linear dependences. Their relationships indicate the changes of the level of the plasma plume non-isothermality along the flow with the increase of the fuel fraction in the initial mixture.

The study of the plasma-liquid system with the discharge in a gas channel with liquid wall in the microporous media under the ultrasound cavitations has shown the following:

• The action of the ultrasound field in the liquid phase increases the efficiency of the nitrous acid production in the work liquid approximately in 1.5 times.

• The ultrasound field in the work liquid influences differently on the content of the emission spectra of discharge plasma. Thus, a part of the emission of OH radicals is reduced comparably to the emission of N_2 molecules. There was a linear increasing of relative intensities of H atoms emission with the time of plasma-liquid processing. But the presence of the ultrasound field reduces this rate approximately in 1.5 times.

The comparison of the developed method of numerical modeling of kinetics in air-water-plasma of atmospheric pressure in the plasma-liquid system in the electrical discharge in the gas channel with liquid wall using the assumption of the averaging of the energy that is deposited in the discharge volume without micro-details of the temporal-spatial structure of the discharge and other method of calculations of plasma kinetics in micro-discharges based on the assumption of the multi-channeling of the current in the plasma volume has shown that both approaches give good results in calculations of the component content and concentrations of main components.

The main components of syngas produced from ethanol in the PLS-DGCLW reactor are molecular hydrogen H_2 and carbon monoxide CO, which relative yield is many times higher than for hydrocarbons CH_4, C_2H_2, C_2H4, and C_2H_6.

The composition content of syngas and the power inputs on the ethanol conversion in the DGCLW discharge depends on the initial gas that forms the plasma and on the ethanol-water ratio in the solution. The output hydrogen concentration grows linearly with discharge current.

The kinetic plasma-chemical modeling is in a fairly good agreement with experimental data, at least, for the main syngas components, H_2 and CO, predicting a non-thermal

plasmachemical mechanism of the ethanol conversion in the investigated plasma-liquid system.

The combination of electric discharge plasma-assisted ethanol reforming and post-dischargepyrolysis of ethanol for hydrogen-rich syngas production is proposed and tested.

The synergetic effect of increasing of total energy efficiency of fuel reforming is demonstrated. PLS system with the glow discharge in the reverse vortex flow of Tornado type with the liquid electrode is proposed and tested. Preliminary results of plasma-assisted reforming of ethanol-water solutions have demonstrated rather high efficiency of fuel conversion and energy transformation.

Kinetics in "tornado" type electrical discharge in ethanol/water/air mixture in the discharge and post-discharge regions were investigated. It was shown, that the ethanol conversion was taking place at both regions. The discharge region acts as a catalyst for the generation of active species (O, OH, H, etc), gas heating and ethanol/water conversion into molecular hydrogen, carbon oxides and hydrocarbons C_xH_y. In the post-discharge region the conversion of ethanol continues, with the additional process of conversion of hydrocarbons C_xH_y.

Numerical simulation of kinetics showed, that the main channels of H_2 generation in plasma were ethanol abstraction for the first 10-100 µs, and hydrocarbons abstraction afterwards. Additionally, the conditions when the reaction between H_2O and hydrogen atoms was the main channel of H_2 production were found.

A kinetic mechanism, which used to describe adequately the chemistry of main components, was proposed. The model did not account for nitrogen-containing species, and nitrogen was considered only as a third body in recombination and dissociation reactions. The comparison between experiments and calculations showed, that the mechanism can describe adequately the concentrations of the main components (H_2, CO, CO_2, CH_4, C_2H_4, C_2H_6 and C_2H_2). Sensitivity analysis for the two main components (H_2 and CO) revealed the most important chemical reactions.

The highest hydrogen yield was reached when concentration of ethanol in the solution was 13%. However, the use of post-discharge region was more beneficial at 6.5% C_2H_5OH concentration, because it increased [H_2] by 30% as compared to the discharge region. Additionally, this regime had the highest conversion rate among the investigated regimes. At the same time, the plasma reactor had the highest efficiency when the concentration of ethanol in the solution was 26%.

Future Work

We are planning the following research activities in the future:

- To study the regimes and parameters of non-thermal plasma reforming of liquid fuels in the pulsed discharge in a gas channel with liquid wall.
- To study the regimes and parameters of non-thermal plasma reforming of liquid fuels in the plasma-liquid system with reverse vortex flow using pulse and DC discharge of tornado type with "liquid" electrode.
- To study the reforming of liquid hydrocarbons in plasma-liquid systems with microporous media (liquid + microbubbles) and aerosols (gas + microdroplets) using low-frequency (~20 kHz) and high-frequency (~800 kHz) ultrasound.
- To study the regimes and parameters of plasma-supported combustion of paraffin fuels by using gas dynamic electric discharges.

6. References

AEO2011 Early Release Overview, available on the sight:
    http:// www.eia.gov/forecast/aeo/pdf/0383er(2011).pdf

Bromberg L, Cohn D R, Rabinovich A, Alexeev N, Samokhin A, Hadidi K, Palaia J, Margarit-Bel N (2006). Onboard Plasmatron Hydrogen Production for Improved Vehicles. *MIT Plasma Science and Fusion Centre*, (February 6 2006), PSFC JA-06-3 (173 pp).

Buchnev V V, Koval S D, Chernyak V Ya (2000). Nonequilibrium arc plasma in transverse air flow. *Bull. Univ. of Kyiv: Series: Phys. & Math.,* No 1, pp. 315-319, ISSN: 1812-5409.

Chernyak V Ya, Naumov V V, Yukhymenko V V, Babich I L, Zrazhevskyy V A, Voevoda Yu V, Pashko T V (2005). Arc discharge in a cross flow of gas. *Probl. Atom. Sci. Technol., Ser. Plasma Phys.*, Vol. 11, No 2, pp. 164-166, ISSN: 1562-6016.

Chernyak V Ya, Yukhymenko V V, Slyusarenko Y I, Solomenko E, Olshevskii S V, Prisyazhnevich I V, Naumov V V, Lukyanchikov V, Demchina V P, Kudryavtsev V S (2007). Plasma conversion of ethanol. *Ind. Heat Eng.*, Vol. 29, No 7, pp. 165-169, ISSN: 0204-3602.

Chernyak V. Ya., Olszewski S. V., Yukhymenko V. V., Solomenko E. V., Prysiazhnevych I V, Naumov V V, Levko D S, Shchedrin A I, Ryabtsev A V, Demchina V P, Kudryavtsev V S, Martysh E V, and Verovchuck M.A. (2008). Plasma-Assisted Reforming of Ethanol in Dynamic Plasma-Liquid System: Experiments and Modeling. *IEEE Trans. Plasma Sci.* Vol.36, No 6, pp.2933-2939, ISSN: 0093-3813.

Dagaout P, Togbe C.2008. Experimental and Modeling Study of the Kinetics of Oxidation of Ethanol−Gasoline Surrogate Mixtures (E85 Surrogate) in a Jet-Stirred Reactor. *Energy & Fuels*, Vol.22, No 5, (July 2008), pp.3499-3505.

Dunphy M P, Patterson P M, Simmie J M 1991. High-temperature oxidation of ethanol. Part 2.—Kinetic modeling, *Journal of the Chemical Society, Faraday Transactions*, Vol.87, No 16, pp.2549-2559.

Fridman A (2008). *Plasma Chemistry* (Cambridge: Cambridge University Press), ISBN-10: 0521847354.

Frenkel Ya. I., 1975. *Kinetic theory of liquids* (Moscow, Nauka).

Held T J, Dryer F L 1998 A comprehensive mechanism for methanol oxidation. *International Journal of Chemical Kinetics*, Vol.30, No11, pp.805-830. ISSN: 1097-4601.

Kakami A., Egawa T., Yamamoto N., Tachibana T., 2010. Plasma-assisted combustion of N_2O/Ethanol propellant for Space Propulsion, *Proceedings of 46th AIAA/ASME/SAE/ASEE Joint Propulsion Conference,* (5 - 28 July 2010), Nashville.

Konnov A. 2008. Remaining uncertainties in the kinetic mechanism of hydrogen combustion. *Combustion and Flame.* Vol.152, No 4, (March 2008), pp.507-528. ISSN: 0010-2180.
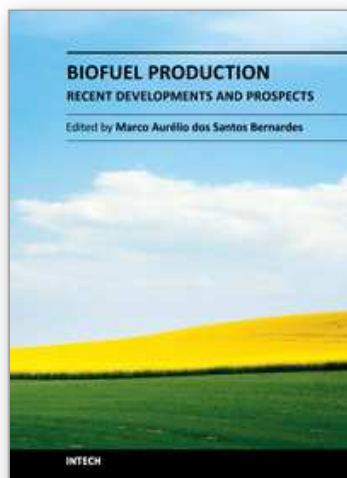
Kosarev I N, Aleksandrov N L, Kindysheva S V, Starikovskaia S M and Starikovskii A Yu 2008 Kinetic mechanism of plasma-assisted ignition of hydrocarbons. *J. Phys. D: Appl. Phys.* 41 No 3 (7 February 2008) 032002 (6pp). ISSN 0022-3727.

Levin D A, Laux C O, Kruger C H 1999. A general model for the spectral calculation of OH radiation in the ultraviolet. *J. Quant. Spectrosc. Radiat. Transfer*. Vol. 61, No 3. pp.377-392, ISSN: 0022-4073.

Levko D S, Shchedrin A I, Chernyak V Ya, Olszewski S V 2010.The effectivity of ethanol conversion in thermal and non-thermal plasma, *Technical Physics* , Vol.80, No 11, pp.152-155, ISSN: 1063-7842.

Marinov N. M. (1999). A detailed chemical kinetic model for high temperature ethanol oxidation. *International Journal of Chemical Kinetics*, Vol.31, No 3, pp. 183-220, ISSN: 1097-4601.

Matveev I.B., Rosocha L.A. (eds.) (2007). Special issue on plasma-assisted combustion. *IEEE Trans. Plasma Sci.*, Vol. 35, No 6, pp. 1605-1606, ISSN: 0093-3813.

Navratil Z., Trunek D., Smid R., Lazar L. (2006). A software for optical emission spectroscopy – problem formulation and application to plasma diagnostics. *Czechoslovak J. Phys.* Vol. 56, No suppl. B, pp.944-951, ISSN: 0011-4626.

NIST Standard Reference Databases Online. Available: http://www.nist.gov/srd/

Petitpas G, Rollier J-D, Darmon A, Gonzales-Aguilar J, Metkemeijer R, Fulcheri L (2007). A comparative study of non-thermal plasma assisted reforming technologies. *Int. J. Hydrogen Energy*, Vol. 32, No 14, pp. 2848-2867, ISSN: 360-3199.

Prieto G, Okumoto M, Shimano K, Takashima K, Katsura S, Mizuno A (2001). Reforming of heavy oil using non-thermal plasma. *IEEE Trans. Ind. Appl.*, Vol. 37, No 5, pp. 1464-1467, ISSN: 0093-9994.

Prysiazhnevych I.V., Chernyak V.Ya., Yukhymenko V.V., Olszewski S.V., Lisitchenko T.E. (2009). Emission spectroscopy of transversal atmospheric pressure discharges. *Problems of Atomic Science and Technology.* Vol. 15 (Series: Plasma Physics), № 1, pp.168-170.

Raizer Yu.P. (1997). *Gas Discharge Physics* (Berlin, Springer-Verlag), ISBN-10: 3540194622.

Shchedrin A. I., Levko D. S., Chernyak V. Ya, Yukhymenko V. V, Naumov V. V., 2008. Effect of air on the concentration of molecular hydrogen in the conversion of ethanol by a non-equilibrium gas-discharge plasma. *JETP Lett*. Vol. 88, No 2,pp. 99-102, ISSN: 0021-3640.

Shchedrin A. group Web site. Available: http://www.iop.kiev.ua/~plasmachemgroup

SPECAIR. Available: http://www.specair-radiation.net/

Shchedrin A I, Levko D S, Chernyak V Ya, Yukhymenko V V, and Naumov V V 2009.Conversion of air mixture with ethanol and water vapors in nonequilibrium gas-discharge plasma.*Technical Physics Lett.* Vol. 35, No 5, (May 2009), pp. 449-451. ISSN: 1063-7850.

Soloshenko I. A., Tsiolko V. V., Pogulay S. S., Terent'eva A. G., Bazhenov V. Yu., Shchedrin A. I., Ryabtsev A. V. and Kuzmichev A. I. 2007. The component content of active particles in a plasma-chemical reactor based on volume barrier discharge. *Plasma Sources Sci. Technol.* Vol.16, No 1, (February 2007), pp.56-87, ISSN 0963-0252.

Wang F, Liu J B, Lee C L, Ronney O D, Gundersen M A (2004). Effect of fuel type on flame ignition by transient plasma discharges. *42nd AIAA Aerospace Sci. Meeting & Exhibit*, (5 - 8 January 2004), Reno, Nevada, AIAA Paper 2004-0837 (10pp), ISSN: 1533-385X.

Yukhymenko V.V., Chernyak V.Ya., Naumov V.V., Veremij Yu.P., Zrazhevskij V. A. (2007). Combustion of ethanol + air mixture supported by transverse arc plasma. *Probl. Atom. Sci. Technol.*, *Ser. Plasma Phys.*, Vol. 13, No 1, pp. 142-144, ISSN: 1562-6016.

Biofuel Production-Recent Developments and Prospects

Edited by Dr. Marco Aurelio Dos Santos Bernardes

This book aspires to be a comprehensive summary of current biofuels issues and thereby contribute to the understanding of this important topic. Readers will find themes including biofuels development efforts, their implications for the food industry, current and future biofuels crops, the successful Brazilian ethanol program, insights of the first, second, third and fourth biofuel generations, advanced biofuel production techniques, related waste treatment, emissions and environmental impacts, water consumption, produced allergens and toxins. Additionally, the biofuel policy discussion is expected to be continuing in the foreseeable future and the reading of the biofuels features dealt with in this book, are recommended for anyone interested in understanding this diverse and developing theme.

How to reference

In order to correctly reference this scholarly work, feel free to copy and paste the following:

Valeriy Ya. Chernyak, Eugen V. Martysh, Sergei V. Olszewski, Vitalij V. Yukhymenko, Sergei M. Sidoruk, Oleg A. Nedybaliuk, Iryna V. Prysiazhnevych, Anatolij I. Shchedrin and Dmitry S. Levko (2011). Ethanol Reforming in the Dynamic Plasma - Liquid Systems, Biofuel Production-Recent Developments and Prospects, Dr. Marco Aurelio Dos Santos Bernardes (Ed.), ISBN: 978-953-307-478-8, InTech, Available from: http://www.intechopen.com/books/biofuel-production-recent-developments-and-prospects/ethanol-reforming-in-the-dynamic-plasma-liquid-systems

INTECH
open science | open minds